processes

MDPI

Article

Comprehensive Assessment of Paleogene Hydrocarbon Source Rocks in the Hydrocarbon-Rich Sub-Sag of the Zhu-1 Depression

Junyan Zhan [1], Guosheng Xu [1,*], Yuling Shi [2], Wanlin Xiong [2] and Shengli Niu [2]

[1] State Key Laboratory of Oil and Gas Reservoir Geology and Exploitation, Chengdu University of Technology, Chengdu 610059, China; zjy19910131@126.com
[2] CNOOC (China) Co., Ltd., Shenzhen Branch, Shenzhen 518054, China
* Correspondence: xgs@cdut.edu.cn; Tel.: +86-13880020853

Abstract: There are two sets of hydrocarbon source rock formations developed in the Paleogene of the Zhu-1 Depression: the Wenchang Formation of semi deep lacustrine facies and the Enping Formation of lacustrine facies. Their basic geochemical characteristics, chemical structures, kerogen components, sedimentary paleoenvironments, etc., are not the same. High quality hydrocarbon source rocks are the basic conditions for oil and gas generation. This article comprehensively evaluates the key depression Paleogene hydrocarbon source rocks in the Zhu-1 Depression, and studies the development mechanism and controlling factors of hydrocarbon source rocks in this area, which is of great significance for understanding the development conditions, quality, and predicting potential high-quality hydrocarbon source rocks. After conducting rock pyrolysis, major and trace element analysis, and infrared spectroscopy experiments on the samples, it was found that the main source rock type of the Wenchang Formation is type II_1, which has a high HI value; the Enping Formation is mainly composed of II_2-III types with low HI values (with a small number of II_1 types), and the source rocks of the Wenchang Formation have a strong hydrocarbon producing aliphatic structure, with the sapropelic and shell formations being larger than the Enping Formation source rocks. By using methods such as CIA values, C values, and Mo-U covariant models, it can be concluded that during the Wenchang to Enping periods, the climate changed from warm and dry to cool and humid, and the overall environment was characterized by freshwater, weak oxidation weak reduction, and gradually decreasing paleo-productivity. At the same time, it was analyzed that the formation of organic rich sediments in the source rocks of the Zhu-1 Depression played an important role in the relative oxygen phase. The ratio of V/(V + Ni) to V/Cr can better indicate the redox environment of the water body and show a good correlation with TOC. Two sets of development models of source rocks controlled by paleooxygen phase were initially established, providing sufficient scientific basis for oil and gas exploration in the area.

Keywords: Zhu-1 depression; Paleogene; hydrocarbon source rocks; paleoenvironment; major and trace elements; infrared spectrum

check for updates

Academic Editor: Qingbang Meng

Received: 29 December 2024
Revised: 28 February 2025
Accepted: 14 March 2025
Published: 20 March 2025

Citation: Zhan, J.; Xu, G.; Shi, Y.; Xiong, W.; Niu, S. Comprehensive Assessment of Paleogene Hydrocarbon Source Rocks in the Hydrocarbon-Rich Sub-Sag of the Zhu-1 Depression. *Processes* **2025**, *13*, 914. https://doi.org/10.3390/pr13030914

Copyright: © 2025 by the authors. Licensee MDPI, Basel, Switzerland. This article is an open access article distributed under the terms and conditions of the Creative Commons Attribution (CC BY) license (https://creativecommons.org/licenses/by/4.0/).

1. Introduction

Since the early 1980s, the Pearl River Mouth Basin has undergone four major comprehensive studies, which have yielded a series of insights of significant importance for oil and gas exploration and resource evaluation in the basin. In 1981, the "Early Oil and Gas Resource Assessment of the Pearl River Mouth Basin" provided initial insights into its exploration potential. Building upon this, the "Reevaluation of Oil and Gas Resources in

the Pearl River Mouth Basin" in 1993 achieved several research outcomes: the development of basin simulation programs for hydrocarbon evaluation and resource estimation, seismic stratigraphic studies in the Huizhou Depression, and the identification of the Huizhou Depression as a hydrocarbon-rich depression, thus defining exploration directions. Subsequently, the "Study on Oil and Gas Accumulation Conditions in the Pearl River Mouth Basin" in 1998 obtained key insights such as the determination of hydrocarbon-rich depressions for oil exploration. This phase summarized twenty years of research and exploration achievements in the Pearl River Mouth Basin. Through the "Study on the Paleogene Half-Graben Reservoir and Exploration Potential in the Zhu-I Depression" in 2007, it was proposed that the Enping Formation primarily contains gas, serving as the main target layer for condensate oil and gas exploration in the Zhu-I Depression. The total resource volume of the three hydrocarbon-rich sags (EP sag, XJ sag, HZ sag) identified during this phase guided exploration in the new Paleogene areas of the Zhu-I Depression.

Oil and gas exploration endeavors in the eastern shallow waters of the Pearl River Mouth Basin have yielded significant results, leading to the establishment of an oil enrichment zone in the northern shelf region, prominently featuring the EP-YJ, XJ, HZ, and LF oilfields, alongside the LH oilfields. Conventional perspectives suggest that, in contrast to the deep-water regions, the Zhu-1 Depression exhibits a lower geothermal gradient and diminished heat flow, thus limiting the thermal evolution of organic matter and consequently, oil generation. However, the discovery of the "26-6" and "Shuanggu" condensate gas reservoirs within the HZ sag, alongside the identification of multiple high gas–oil ratio reservoirs, challenges the traditional understanding. These findings not only defy conventional wisdom but also expand the horizons for natural gas exploration within oil-type basins.

Due to their relatively small catchment areas and higher sensitivity to external environmental changes, lacustrine hydrocarbon source rocks exhibit strong heterogeneity [1]. The formation of lacustrine hydrocarbon source rocks requires an optimal combination of tectonic processes, climatic conditions, and environmental characteristics. However, the development mechanism of lacustrine hydrocarbon source rocks has been a topic of debate among researchers. Based on different samples and analytical methods, scholars have proposed various factors controlling the development of source rocks. These factors can be summarized as primarily influencing ancient productivity [2], organic matter preservation conditions [3], and sedimentation rates of sediments [4]. Due to significant disparities in paleoclimatic, structural, and paleolimnological characteristics between the middle-deep lacustrine Wenchang Formation and the lacustrine-marsh Enping Formation within the Zhu-1 Depression, some scholars have attributed the differential enrichment of oil and gas to variances in the properties of these formations' source rocks [5]. Source rocks play a pivotal role in governing the formation and distribution of terrestrial petroleum. However, the developmental mechanisms and controlling factors influencing the source rocks of the Wenchang Formation and the Enping Formation remain poorly understood. Hence, investigating the developmental mechanisms and controlling factors of source rocks in the Zhu-1 Depression, and establishing a development model for the Wenchang Formation and the Enping Formation, hold significant theoretical importance in comprehending the mechanisms underlying the differential enrichment of oil and gas. Moreover, it carries essential practical implications for optimizing exploration strategies and mitigating exploration risks. This study primarily focused on four key sub-sags: "HZ-A sub-sag", "HZ-B sub-sag", "EP-A sub-sag", and "XJ-A sub-sag".

For the first time, this research clearly demonstrates that the organic matter enrichment of source rocks within the Enping Formation and Wenchang Formation in the Zhu-1 Depression is governed by the same ancient oxygen phase. The ratio of V/(V + Ni) to V/Cr

can serve as a better indicator of the redox environment of the water body and exhibits a strong correlation with TOC.

2. Geological Background

Located at the junction of the Indian, Pacific, and Eurasian plates, the Pearl River Mouth Basin is a Cenozoic rift basin formed on the complex folded Paleozoic and Mesozoic basement [6,7]. It is composed of five tectonic units, the northern uplift zone, the northern depression zone (Zhu 1 and Zhu 3 Depressions), the central uplift zone, the southern depression zone (Zhu 2 Depression) and the southern uplift zone [8]. The Zhu 1 Depression in the northern depression zone of the Pearl River Mouth Basin [9] is bounded by the northern uplift zone in the north, the Panyu low uplift and the Dongsha uplift in the south, and the Zhu 3 Depression in the west, and includes five negative tectonic units, which from west to east are the EP sag, XJ sag, HZ sag, LF sag and HJ sag (Figure 1).

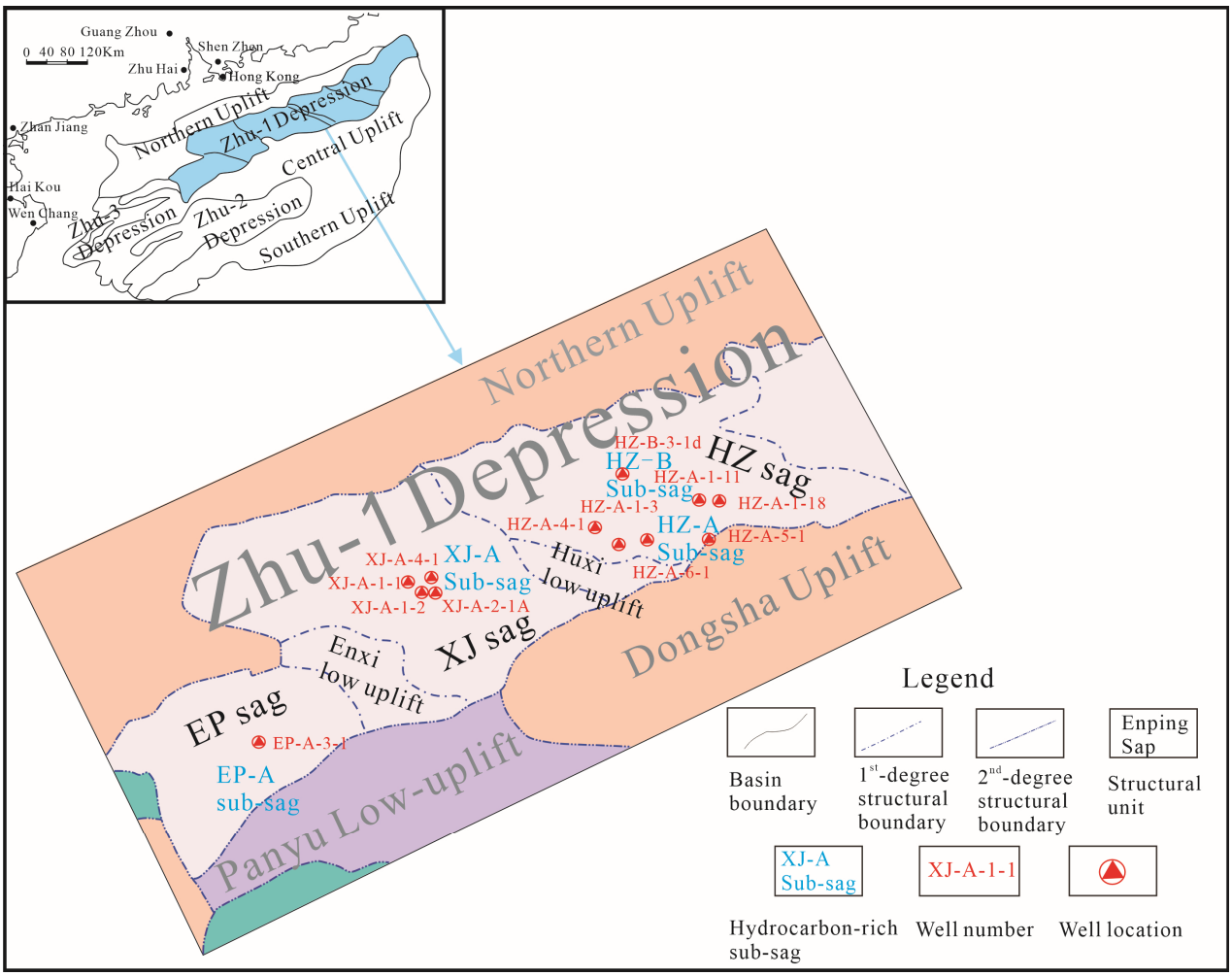


Figure 1. Tectonic pattern of the Pearl River Mouth Basin.

During the Mesozoic era, the Pearl River Mouth Basin experienced compressional accretionary activity, akin to the Andean continental margin. Extensive faulting and magmatic events occurred throughout the Yanshan period, reshaping the basin's structure and pre-existing Paleozoic basement. Notably, the third phase of the Yanshan Mountains saw the eruption of intermediate acidic magma, forming the South China granite and volcanic rock belt. Tectonic stresses led to a dynamic tectonic framework governed by the Neocathaysian and Middle Tethyan systems. After the Late Cretaceous period, the

Pacific Plate's movement slowed, transitioning China's eastern margin to tension and the southern margin to passive. This shift caused the crust to thin and extended the continental margin into the ocean. Sediments from the Late Baili to Eocene periods were primarily terrigenous clastic rocks. The Lower Oligocene Enping Formation comprised faulted lake, swamp, river, and delta deposits. Later, marine transgression deposited marine strata in the Quaternary Pearl River Formation. The eastern basin experienced block fault uplift and volcanic activity during the middle and late Miocene periods.

The Pearl River Mouth Basin has successively experienced tectonic movements, such as the Shenhu Movement, the first episode of the Zhuqiong Movement, the second episode of the Zhuhai Formation, the South China Sea Movement and the Baiyun Movement. The strata are distributed from bottom to top, including the Shenhu Formation, Wenchang Formation, Enping Formation, Zhuhai Formation, Zhujiang Formation, Hanjiang Formation, Yuehai Formation, and Wanshan Formation. The Paleogene mainly developed the lower faulted layers of the rift period, including two main sets of high-quality hydrocarbon-forming layers: the Wenchang Formation (six third-order sequences) and the Enping Formation (four third-order sequences) [10] (Figure 2).

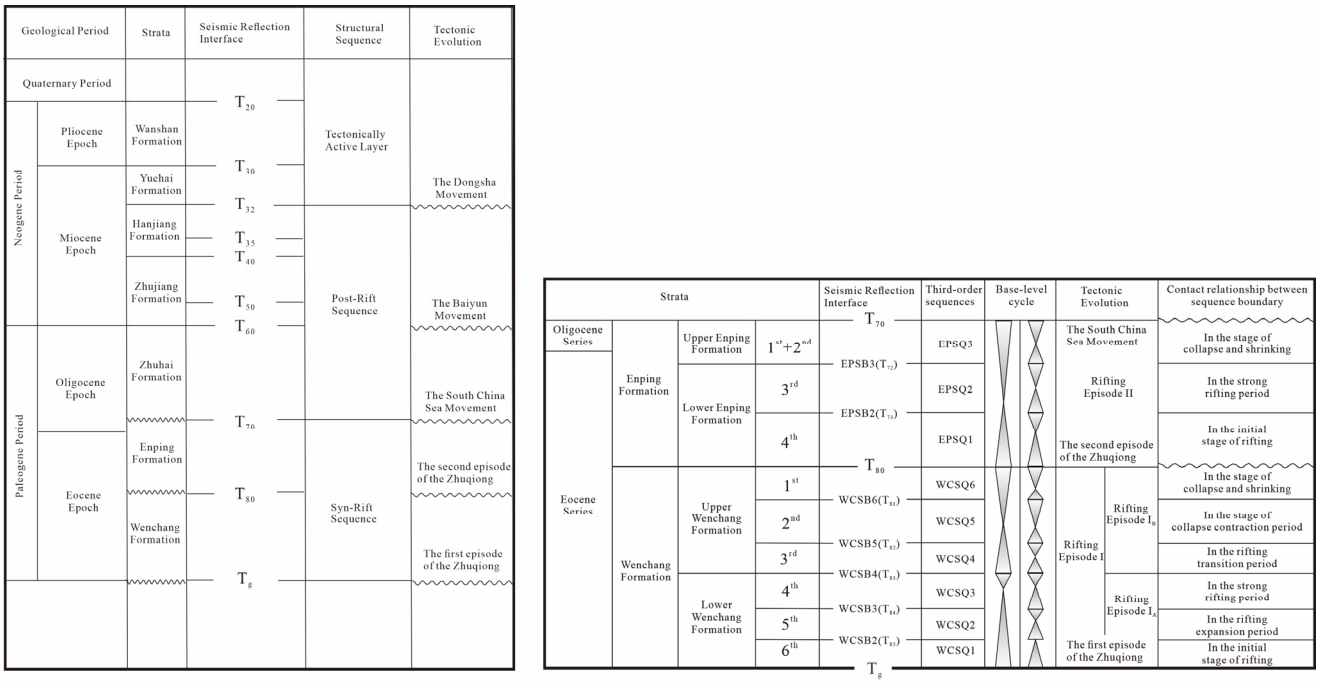


Figure 2. Stratigraphic grid in Zhu I depression of the Pearl River Mouth Basin.

The Wenchang Formation was formed during a significant rift phase in the basin, showing a clear change from the underlying Shenhu Formation. It began with the T90 reflector and ended with the uplift of the fault depression, causing erosion and creating the T80 reflector, indicating a widespread unconformity. The formation's sedimentary centers reached over 1000 m in thickness, with deep lacustrine deposits dominating the center and shallow lacustrine deposits surrounding it. The Enping Formation, deposited during another rift episode, shows distinct contacts with underlying strata and appears as the T80 unconformity surface. In areas with basement uplift, it directly overlays the basement. Towards the end of its deposition, regional uplift and erosion, influenced by the South China Sea movement, created the T70 unconformity surface. The formation's thickness varies but typically exceeds 1000 m, with lacustrine deposits in the center and fluvial deposits along the margins. The Enping Formation is an important source rock within the Zhu-1 Depression.

The Pearl River Mouth Basin in China is significant for its oil and gas reserves, primarily sourced from the Wenchang Formation and the Enping Formation. The Wenchang Formation's lacustrine oil-type hydrocarbon source rocks, formed during the early-middle rift period, are crucial contributors to hydrocarbon accumulation. Conversely, the Enping Formation's coal-measure hydrocarbon source rocks, from the late rifting period, have a lower contribution [11]. Biomarker compositions differ significantly between the two formations [12–14]. The Wenchang Formation has an average total organic carbon (TOC) of 2.06%, while the Enping Formation's TOC averages 1.91%. Zhu et al. [15] revealed high oil and gas production rates from Paleogene hydrocarbon source rocks, with the Wenchang Formation exhibiting higher rates compared to the Enping Formation. The study area, especially the eastern shallow water area, holds mature to highly mature Paleogene hydrocarbon source rocks, with the main hydrocarbon formation period dating back to 16 million years ago. Oil and gas resources in the Zhu-1 Depression are significant, with billions of tons of oil and millions of tons of natural gas reserves in various sags, according to the second national resource assessment [16].

3. Samples and Methods

Representative drilling wells were selected in the study area to drill a large set of continuous mudstone intervals of the Enping Formation and Wenchang Formation hydrocarbon source rocks. Based on different sedimentary facies and different layers, the major and trace elements, total organic carbon, rock pyrolysis, infrared spectroscopy were comprehensively designed and studied. The sampling quantity is shown in the following Table 1.

Table 1. Sampling quantity from the hydrocarbon-rich sub-sag of the Zhu-1 Depression.

	Rock–Eval Pyrolysis	Major and Trace Elements	Infrared Spectrum	Microscopic Components
HZ-A	62	35	15	15
HZ-B	49	/	/	/
EP-A	31	11	6	6
XJ-A	54	25	9	9

3.1. Rock–Eval Pyrolysis

The preparation of samples for TOC analysis followed the procedures specified in GB/T 19145-2003 (Chinese national standard) [17]. A total of 10 g of sample was ground to 80 mesh using a pestle and agate mortar. Samples were digested in hydrochloric acid (5%) for 2 h to remove carbonate minerals, and the acid was removed with distilled water. Then, the samples were dried in an oven at 60 °C. The TOC of the samples was measured using a Leco CS-230 carbon-sulfur analyzer (LECO Instruments Company Limited, Beijing, China). The accuracy is within 0.5%. According to the detailed procedures of GB/T 18602-2012 (Chinese national standard) [18], rock samples were pulverized to 160 mesh and then dried in an oven. Rock Eval pyrolysis was performed on these powdered samples using a Rock Eval II instrument (IFPEN, Rueil Malmaison, France). Free hydrocarbons (S_1) were measured at 300 °C (3 min). When the sample was heated from 300 °C to 550 °C at a rate of 25 °C/min, hydrocarbons (S_2) were generated. The carbon dioxide production rate (S_3) was obtained when the sample was heated from 300 °C to 550 °C at 25 °C/min. The temperature at the maximum pyrolysis product yield (Tmax) was determined when S_2 reached its maximum yield.

3.2. Analysis of Major and Trace Elements

Grind the sample into a powder smaller than 200 mesh and then divide it into two parts (one for major element analysis and the other for trace element analysis). In order to analyze the main elements, the samples were heated in a muffle furnace at 1000 °C for 1 h. Three samples were weighed from each sample. The first sample was digested with perchloric acid, nitric acid, hydrofluoric acid, and hydrochloric acid, heated and evaporated to near dryness, and finally dissolved in dilute hydrochloric acid to a certain volume. The S-Ca-Fe-Mn-Cr content was roughly measured using plasma emission spectroscopy (ICP-AES) to confirm the suitability of the selected XRF process. Take another sample and dry it at 105 °C, accurately weigh the sample mass, place it in a platinum crucible, add lithium tetraborate lithium metaborate lithium nitrate mixed flux, confirm that the sample and flux are fully mixed, melt it with a high-precision melting machine at 1050 °C, pour the melt into a platinum mold, cool it to form a melt, confirm that the quality of the melt is qualified (if the melt is unqualified, it must be re weighed and melted), and then use an X-ray fluorescence spectrometer to measure the content of the main elements. To ensure testing accuracy, larger platinum molds are used. At the same time, accurately weigh the third dried sample, burn it in an oxygen furnace at 1000 °C, and accurately weigh the mass of the cooled sample. The difference in mass before and after burning the sample is the loss on ignition (LOI). The sum of loss on ignition (LOI) and element content measured by XRF (total amount expressed as oxide) is called "total". For conventional samples, the sum is approximately 100% (99.01~100.99%). The steps for trace element analysis (such as Sr, Ba, V, Ni, U, Mo, Cr) are as follows. Weigh two samples, add perchloric acid, nitric acid, and hydrofluoric acid to the first sample for digestion, heat and evaporate to near dryness, then dissolve the sample in dilute hydrochloric acid to a constant volume, and finally analyze it using plasma emission spectroscopy and plasma mass spectrometry. The second sample is added to lithium metaborate/lithium tetraborate flux, mixed evenly, and melted in a furnace above 1025 °C. After cooling, the melt is diluted with a mixture of nitric acid, hydrochloric acid, and hydrofluoric acid, and then analyzed using a plasma mass spectrometer. Based on the actual situation and digestion effect of the sample, select the test results after comprehensive analysis. Before the experiment, test blank samples for each sample to ensure accuracy. The relative standard deviation of major and trace elements is less than 5%. The detailed procedures for principal and trace element analysis follow the Chinese national standards GB/T 14506.14-2010 [19] and GB/T 14506.30-2010 [20], respectively.

3.3. Al Normalization

Trace elements usually need to be normalized by Al to correct the dilution from organics and native minerals [21,22]. Algeo and Maynard [23] found that if Al is mainly present in siliceous clastic phases and is immobile in the diagenetic environment, the Al normalization is effective. The normalized formula of Al is given as follows:

$$EF_{element}\ X = (X_{sample}/Al_{sample})/(X_{background}/Al_{background}) \quad (1)$$

Here, X_{sample} and Al_{sample} represent the contents of X and Al in the sample, respectively. $X_{background}$ and $Al_{background}$ are the average contents of the Archean Australian shale (PAAS) after Taylor and McLennan [24]. If $EF_{element}$ X < 1 is relatively no enrichment in PAAS, $EF_{element}$ X > 1 is relative enrichment, $EF_{element}$ X > 3 is equivalent to detectable spontaneous enrichment, and $EF_{element}$ X > 10 is equivalent to strong enrichment [25].

3.4. Infrared Spectrum and Microscopic Components

The measurement spectrum was in the range of 4000~40 cm^{-1}, the resolution was 4 cm^{-1}, the grating aperture was 34 mm, the scans were 120 times, and the scan rate was 0.6829 cm/s. The difference in composition and structure between samples can be quantitatively compared based on the absorption intensity of infrared spectrum. Therefore, the accuracy of infrared absorption spectrum is particularly important. During the experiment, (1 ± 0.005) mg kerogen was weighed, and the diluted sample was placed in an agate mortar according to the dilution mass ratio of kerogen to potassium bromide (1:100) until the spectrum of the sample met the requirements. Affected by the number of grindings, the homogeneous grinding material was taken out and pressed into thin slices under vacuum pressure of 10 MPa for 2 min. Then, the flakes were dried in the vacuum drying oven for 48 h to reduce the moisture interference with the chromatograms.

The identification of minerals and organic matter using light transmission, polarization, reflection, and fluorescence under a MF43 transmission reflection polarized fluorescence microscope (Guangzhou Mingmei Optoelectronic Technology Co., Ltd., Guangzhou, China) is based on SY/T6414-2014 "Identification and Statistical Methods for Microscopic Components of Whole Rock Light Slices".

4. Results

4.1. Geochemical Characteristics of Source Rocks

Table 2 lists the geochemical parameter information of the rocks. Peter [26] believed that Tmax in rock pyrolysis could effectively reflect the maturity of hydrocarbon source rocks. The Tmax value of the Enping Formation samples in this experiment was 360–463 °C, with an average of 442.35 °C. The Tmax value of the Wenchang Formation samples was in the range of 366–481 °C, with an average of 427.67 °C. Although a small number of samples are in the immature-low mature stage, the Enping Formation hydrocarbon source rocks have entered the mature stage, and the current is the peak oil generation period; the Wenchang Formation hydrocarbon source rocks have reached the mature-high maturity stage, indicating the oil and gas symbiosis stage [27].

The relationship diagram of hydrogen index (HI) and Tmax proposed by Tissot and Welte [28] was used to determine the kerogen type. At present, only the periphery of the HZ-A sub-sag has encountered the typical hydrocarbon source rocks of the early-middle rift Wenchang Formation (XJ-A sub-sag, the Wenchang Formation in EP-A sub-sag is not representative), the types are mainly type II_1 and have a high HI (46.00–483.35, average 229.79); the Enping Formation (data based on dark mudstone and not including coal measure) is an important hydrocarbon source rock in the Zhu-1 Depression, which has been drilled in every sub-sag, mainly types II_2-III (with a small part of type II_1), and the HI is not high (22.61–332.00, average 158.15, Figure 3a–d).

According to the classification standards of hydrocarbon source rocks in Chinese lakes [29], the quality of hydrocarbon source rocks can be divided into non-hydrocarbon source rocks and poor, moderate, good, and very good hydrocarbon source rocks. The hydrocarbon source rocks of the Wenchang Formation have high organic matter abundance and have High TOC value (0.50–5.48%, average 2.23%) and S_1 + S_2 (0.59–26.76 mg/g, average 8.23 mg/g); the hydrocarbon source rocks of the Enping Formation were mainly poor-medium quality, the TOC value was higher (0.29–9.61%, 1.44% on average) but the S_1 + S_2 (0.20–21.68 mg/g, average 2.98 mg/g) was lower; however, the quality of each sub-sag was slightly different: the XJ-A sub-sag was the best, followed by EP-A sub-sag and the HZ-B sub-sag, and the HZ-A sub-sag was the worst (Figure 3e–h).

Table 2. Geochemical parameters of samples from the hydrocarbon-rich sub-sag of the Zhu-1 Depression.

Sub-Sag	Well Number	Strata	Depth m	TOC %	Tmax °C	HI mg/g·TOC	S_1 mg/g	S_2 mg/g	S_3 mg/g	$S_1 + S_2$ mg/g
HZ-A	HZ-A-1-1	Enping formation	3672.50	1.20	450.00	121.67	0.17	1.46	1.83	1.63
			3707.50	3.40	445.00	170.59	0.74	5.80	1.25	6.54
			3847.50	2.60	453.00	170.38	0.55	4.43	1.01	4.98
			3922.50	2.60	450.00	238.85	0.99	6.21	1.23	7.20
			4002.50	1.50	453.00	85.33	0.29	1.28	2.30	1.57
			4081.50	1.80	461.00	107.22	0.26	1.93	2.76	2.19
			4097.50	3.40	458.00	145.59	0.63	4.95	1.25	5.58
			4111.50	1.80	461.00	105.56	0.31	1.90	2.76	2.21
			4126.50	1.40	458.00	99.29	0.24	1.39	2.14	1.63
			4142.50	1.30	463.00	93.85	0.19	1.22	1.99	1.41
			4156.50	1.70	459.00	102.94	0.29	1.75	2.61	2.04
		Wenchang formation	4191.00	1.57	374.00	155.00	0.69	2.44	1.41	3.13
			4206.00	1.46	366.00	181.00	0.84	2.64	1.24	3.48
			4224.00	1.06	378.00	168.00	0.80	1.78	1.61	2.58
			4236.00	1.40	369.00	158.00	0.83	2.21	0.14	3.04
			4254.00	1.50	379.00	145.00	0.97	2.18	2.30	3.15
			4284.00	1.40	379.00	165.00	0.85	2.31	2.14	3.16
			4302.00	1.14	381.00	172.00	1.57	1.96	1.74	3.53
	HZ-A-1-18	Enping formation	3768.00	0.77	405.00	226.00	0.57	1.74	1.16	2.31
			3849.00	1.04	443.00	168.00	0.40	1.75	1.58	2.15
			3876.00	0.34	368.00	279.00	0.22	0.95	0.49	1.17
			3939.00	0.62	410.00	197.00	0.27	1.22	0.93	1.49
			4115.50	0.49	360.00	231.00	0.25	1.13	0.73	1.38
			4155.00	0.34	368.00	262.00	0.16	0.89	0.49	1.05
		Wenchang formation	4191.00	1.57	374.00	155.00	0.69	2.44	2.41	3.13
			4206.00	1.46	366.00	181.00	0.84	2.64	2.24	3.48
			4224.00	1.06	378.00	168.00	0.80	1.78	1.61	2.58
			4236.00	1.40	369.00	158.00	0.83	2.21	2.14	3.04
			4254.00	1.50	379.00	145.00	0.97	2.18	2.30	3.15
			4284.00	1.40	379.00	165.00	0.85	2.31	2.14	3.16
			4302.00	1.14	381.00	172.00	1.57	1.96	1.74	3.53
	HZ-A-4-1	Enping formation	3637.50	0.58	451.00	24.28	0.06	0.14	0.87	0.20
			3661.50	0.36	440.00	44.25	0.10	0.16	0.52	0.26
			3670.50	0.71	454.00	22.61	0.04	0.16	1.07	0.20
			3685.50	0.57	454.00	66.36	0.11	0.38	0.85	0.49
			3688.50	0.62	445.00	51.46	0.10	0.32	0.93	0.42
			3715.50	0.86	450.00	45.38	0.12	0.39	1.30	0.51
	HZ-A-6-1	Wenchang formation	3457.50	3.33	440.00	465.81	3.82	15.49	1.01	19.31
			3460.50	4.13	444.00	467.83	4.46	19.30	0.84	23.76
			3463.50	4.52	442.00	483.35	4.89	21.87	0.88	26.76
			3548.50	3.15	441.00	401.76	3.60	12.67	1.37	16.27
	HZ-A-5-1	Wenchang formation	4578.50	3.67	451.00	282.28	7.64	10.37	8.07	18.01
			4589.50	3.55	449.00	269.83	5.40	9.57	7.01	14.97
			4607.50	4.37	450.00	234.82	4.96	10.27	5.75	15.23
			4622.50	4.44	450.00	255.28	6.13	11.33	6.39	17.46
			4637.50	3.48	447.00	239.33	5.01	8.32	5.94	13.33
			4651.50	2.85	447.00	262.44	4.46	7.49	6.52	11.95
			4662.50	3.99	450.00	243.46	4.42	9.72	5.89	14.14
			4676.50	2.97	448.00	247.96	3.73	7.37	6.30	11.10
	HZ-A-1-3	Wenchang formation	3807.50	3.38	444.00	389.37	2.53	13.17	0.96	15.70
			3817.50	4.56	445.00	431.42	3.78	19.66	1.01	23.44
			3825.50	3.15	438.00	401.42	3.84	12.63	1.43	16.47
			3837.50	3.25	443.00	378.15	3.03	12.29	1.09	15.32
			3855.50	3.42	441.00	366.75	3.54	12.54	1.32	16.08
			3867.50	3.73	439.00	374.53	4.68	13.98	1.26	18.66
			3880.50	3.39	438.00	370.50	4.30	12.55	1.49	16.85
			3894.50	2.50	434.00	380.85	3.09	9.54	1.55	12.63

Table 2. *Cont.*

Sub-Sag	Well Number	Strata	Depth m	TOC %	Tmax °C	HI mg/g·TOC	S_1 mg/g	S_2 mg/g	S_3 mg/g	$S_1 + S_2$ mg/g
HZ-B	HZ-B-3-1d	Enping formation	4683.50	1.40	444.90	177.22	0.56	2.49	1.17	3.05
			4687.00	1.47	448.80	161.76	0.56	2.38	0.28	2.94
			4690.50	0.69	448.40	329.39	0.49	2.28	0.97	2.77
			4692.50	1.21	448.90	64.00	0.23	0.78	1.85	1.01
			4697.00	0.89	450.80	160.32	0.47	1.42	1.30	1.89
			4702.50	0.80	452.60	144.11	0.38	1.15	1.14	1.53
			4706.50	0.80	451.90	157.28	0.48	1.26	1.15	1.73
			4709.00	1.66	439.90	149.07	0.55	2.47	2.59	3.01
			4712.50	2.01	446.70	197.14	0.92	3.96	1.18	4.88
			4717.50	0.78	449.30	150.08	0.37	1.17	1.11	1.54
			4723.00	0.54	455.20	148.72	0.30	0.81	0.72	1.11
			4737.00	0.68	456.60	137.25	0.35	0.93	0.95	1.28
			4742.00	0.29	459.60	152.60	0.19	0.44	0.29	0.63
			4751.00	0.91	457.50	106.86	0.21	0.97	1.34	1.18
			4765.50	0.76	451.20	137.82	0.36	1.05	1.08	1.41
			4772.50	0.67	448.30	145.39	0.35	0.98	0.93	1.33
			4777.50	0.82	454.60	102.22	0.36	0.84	1.18	1.20
			4785.50	0.56	447.10	136.27	0.31	0.76	0.75	1.07
			4793.00	0.63	461.20	99.28	0.26	0.62	0.86	0.89
			4797.00	0.55	453.00	115.46	0.25	0.64	0.74	0.89
			4807.50	0.76	445.90	137.61	0.34	1.04	1.08	1.38
			4812.50	0.54	447.20	139.46	0.29	0.75	0.71	1.04
			4815.50	0.71	449.00	131.16	0.32	0.93	1.00	1.25
			4819.50	0.50	447.20	147.06	0.27	0.74	0.65	1.01
			4825.50	0.58	450.00	123.85	0.27	0.72	0.78	0.99
			4832.00	0.63	458.40	109.76	0.27	0.70	0.87	0.96
			4836.50	0.63	452.30	105.15	0.27	0.67	0.87	0.93
			4839.50	0.56	440.60	135.54	0.32	0.76	0.75	1.08
			4853.50	0.59	454.80	136.92	0.29	0.81	0.79	1.09
			4858.00	0.69	443.50	101.92	0.27	0.70	0.96	0.97
			4870.50	0.50	443.30	127.37	0.28	0.64	0.64	0.91
			4874.50	0.58	438.00	137.21	0.34	0.79	0.78	1.14
			4883.50	0.55	440.40	156.62	0.32	0.86	0.73	1.18
			4887.50	0.71	445.20	97.28	0.33	0.69	0.99	1.02
			4892.50	0.77	441.90	131.12	0.40	1.01	1.11	1.41
			4897.50	0.65	444.80	115.66	0.34	0.75	0.89	1.09
			4910.00	0.55	439.20	151.40	0.31	0.83	0.73	1.14
			4915.50	0.49	447.90	128.83	0.26	0.63	0.62	0.88
			4932.00	0.54	446.00	129.35	0.27	0.70	0.71	0.97
			4936.00	1.05	442.50	79.29	0.34	0.83	1.57	1.17
			4944.00	0.65	450.40	104.38	0.30	0.68	0.90	0.98
			4948.00	0.91	446.70	130.27	0.44	1.19	1.34	1.63
			4955.50	0.58	450.70	149.75	0.33	0.87	0.78	1.20
			4959.00	1.04	446.30	133.26	0.49	1.39	1.55	1.88
			4965.50	0.76	447.60	141.28	0.47	1.07	1.08	1.54
			4970.50	0.92	446.50	132.30	0.45	1.22	1.35	1.67
			4977.00	0.65	439.90	225.23	0.46	1.46	0.89	1.92
			4986.50	0.67	437.00	209.82	0.40	1.41	0.97	1.80
			4999.00	0.57	438.10	213.56	0.36	1.23	0.77	1.58
EP-A	EP-A-3-1	Enping formation	3425.00	0.90	438.00	66.00	0.07	0.59	0.54	0.66
			3432.60	1.46	443.00	95.00	0.18	1.39	0.97	1.57
			3445.00	1.00	440.00	96.00	0.17	0.96	0.74	1.13
			3465.00	1.22	441.00	98.00	0.19	1.19	0.87	1.38
			3535.00	2.36	436.00	172.00	2.20	4.07	2.41	6.27
			3570.00	3.39	440.00	132.00	0.62	4.48	2.63	5.10
			3595.00	0.71	444.00	120.00	0.11	0.85	0.68	0.96
			3687.50	1.16	440.00	289.00	0.46	3.35	2.02	3.81
			3687.50	1.16	440.00	289.00	0.46	3.35	2.02	3.81
			3715.00	0.77	445.00	90.00	0.15	0.69	0.60	0.84
			3850.00	0.55	433.00	105.00	0.15	0.58	0.54	0.73
			3910.00	0.55	447.00	89.00	0.12	0.49	0.49	0.61
			4220.00	0.62	446.00	113.00	0.11	0.70	0.60	0.81
			4292.50	1.58	453.00	207.00	0.87	3.27	1.98	4.14
			4337.50	1.47	455.00	178.00	0.69	2.61	1.63	3.30
			4335.00	1.40	457.00	101.00	0.31	1.42	0.99	1.73
			4350.00	3.64	457.00	158.00	1.11	5.75	3.31	6.86
			4387.50	1.21	452.00	197.00	0.86	2.38	1.50	3.24
			4462.50	9.61	459.00	142.00	1.86	13.65	7.54	15.51
		Wenchang formation	4487.50	3.44	459.00	158.00	1.04	5.43	3.14	6.47
			4480.00	4.20	465.00	120.00	1.07	5.05	2.93	6.12
			4585.00	1.25	470.00	90.00	0.47	1.13	0.83	1.60
			4595.00	1.25	470.00	88.00	0.47	1.10	0.82	1.57
			4637.50	1.25	459.00	116.00	0.48	1.45	1.00	1.93
			4625.00	1.30	475.00	67.00	0.40	0.87	0.69	1.27
			4640.00	0.95	458.00	75.00	0.29	0.71	0.61	1.00
			4645.00	1.02	458.00	86.00	0.38	0.88	0.70	1.26
			4687.50	1.61	473.00	80.00	0.61	1.28	0.91	1.89
			4755.00	0.88	481.00	50.00	0.15	0.44	0.46	0.59
			4765.00	1.45	430.00	73.00	0.36	1.06	0.80	1.42
			4780.00	0.93	479.00	46.00	0.17	0.43	0.46	0.60

Table 2. *Cont.*

Sub-Sag	Well Number	Strata	Depth m	TOC %	Tmax °C	HI mg/g·TOC	S_1 mg/g	S_2 mg/g	S_3 mg/g	$S_1 + S_2$ mg/g
XJ-A	XJ-A-1-1	Enping formation	3952.50	1.00	433.00	325.00	0.54	3.25	1.22	3.79
			3975.00	1.26	432.00	259.00	0.54	3.26	1.21	3.80
			4006.50	1.83	428.00	281.00	0.65	5.15	1.49	5.80
			4033.50	2.03	430.00	262.00	0.77	5.31	1.77	6.08
			4087.50	1.20	435.00	281.00	0.64	3.37	1.46	4.01
			4114.50	2.12	431.00	283.00	1.05	6.00	2.44	7.05
			4132.50	1.17	435.00	255.00	0.39	2.98	0.86	3.37
			4170.00	1.03	427.00	240.00	0.29	2.47	0.62	2.76
			4252.50	1.79	437.00	288.00	0.75	5.15	1.73	5.90
			4302.00	1.03	437.00	268.00	0.55	2.76	1.25	3.31
			4363.50	2.05	440.00	242.00	0.93	4.97	2.16	5.90
			4399.50	4.03	438.00	264.00	1.70	10.64	4.00	12.34
		Wenchang formation	4432.50	3.95	440.00	242.00	1.92	9.55	4.53	11.47
			4435.00	5.48	441.00	269.00	1.54	14.76	3.62	16.30
			4453.50	2.32	443.00	271.00	0.95	6.28	2.20	7.23
			4471.50	1.30	443.00	308.00	0.47	4.00	1.05	4.47
			4507.50	0.50	446.00	334.00	0.27	1.66	0.57	1.93
			4537.50	0.56	443.00	294.00	0.27	1.65	0.37	1.92
			4608.00	0.54	445.00	351.00	0.24	1.88	0.50	2.12
			4692.00	0.62	443.00	313.00	0.31	1.94	0.67	2.25
	XJ-A-1-2	Enping formation	3924.00	0.89	430.00	292.00	0.48	2.60	1.08	3.08
			4101.00	3.43	433.00	332.00	1.95	11.39	4.60	13.34
			4125.00	1.37	434.00	308.00	1.03	4.22	2.40	5.25
			4203.00	0.99	433.00	313.00	0.70	3.10	1.61	3.80
			4383.00	1.62	435.00	286.00	1.29	4.64	3.02	5.93
			4407.00	6.38	439.00	293.00	2.96	18.72	7.02	21.68
			4428.00	5.62	438.00	324.00	3.00	18.22	7.12	21.22
		Wenchang formation	4554.00	0.56	449.00	289.00	0.24	1.62	0.50	1.86
			4617.00	0.56	438.00	382.00	0.36	2.14	0.79	2.50
	XJ-A-2-1A	Enping formation	4089.50	1.57	428.00	157.96	0.25	2.48	2.20	2.73
			4120.50	1.23	434.00	111.81	0.22	1.38	1.14	1.60
			4153.50	1.32	428.00	77.30	0.25	1.02	1.25	1.27
			4188.50	2.62	439.00	108.41	0.38	2.84	0.98	3.22
			4227.50	1.25	438.00	98.05	0.17	1.23	0.64	1.40
			4271.50	1.16	436.00	98.80	0.15	1.15	0.66	1.30
			4302.50	6.63	440.00	154.22	0.84	10.23	0.95	11.07
			4333.50	2.61	440.00	146.29	0.30	3.82	0.39	4.12
			4356.50	2.28	420.00	277.33	2.80	6.33	1.75	9.13
			4389.50	2.36	425.00	252.82	2.03	5.96	2.36	7.99
			4419.50	2.79	441.00	100.17	0.32	2.79	0.28	3.11
			4446.50	2.12	443.00	126.23	0.38	2.67	0.58	3.05
			4480.50	4.05	443.00	108.53	0.65	4.40	1.48	5.05
			4509.50	2.11	449.00	111.21	0.29	2.35	0.41	2.64
			4544.50	2.86	445.00	114.79	0.35	3.28	0.50	3.63
			4572.50	2.16	444.00	128.98	0.30	2.79	0.41	3.09
			4593.50	1.69	448.00	97.40	0.31	1.65	0.37	1.96
			4622.50	1.30	449.00	93.79	0.18	1.22	0.23	1.40
			4655.50	1.58	449.00	100.04	0.24	1.58	0.29	1.82
			4691.50	2.26	451.00	121.12	0.35	2.74	0.31	3.09
	XJ-A-4-1	Enping formation	3554	1.18	443.00	163.00	0.13	1.92	0.24	2.05
			3483	1.30	441.00	135.00	0.31	1.75	0.67	2.06
			3586.5	0.86	439.00	58.00	0.22	1.15	0.45	1.37
			3658.5	0.90	440.00	47.00	0.29	1.27	0.62	1.56
			3693	0.85	446.00	181.00	0.19	1.54	0.38	1.73

Legend: "TOC" means total organic carbon; "Tmax" means the maximum temperature at which hydrocarbons are released during the pyrolysis process; "/"means data not detected; "HI" means Hydrogen Index = ($S_2 \times 100$/TOC); "S_1" means free hydrocarbons; "S_2" means hydrocarbons produced during the pyrolysis process of the rock.

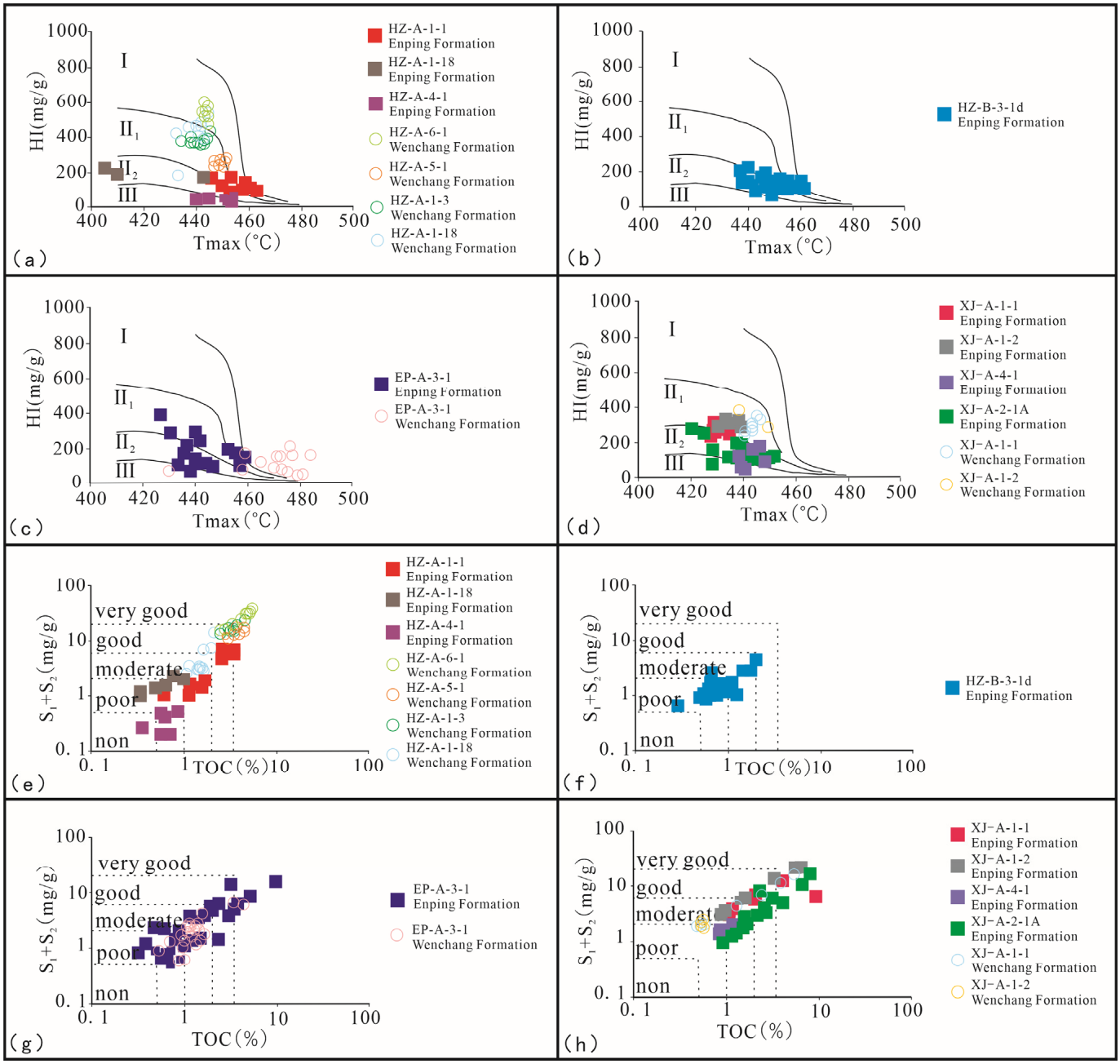


Figure 3. Hydrogen index (HI)-Tmax map and TOC-(S_1 + S_2) diagrams of hydrocarbon source rocks in the Zhu-1 Depression. ((**a**) HZ-A sub-sag, (**b**) HZ-B sub-sag, (**c**) EP-A sub-sag, (**d**) XJ-A sub-sag, (**e**) HZ-A sub-sag, (**f**) HZ-B sub-sag, (**g**) EP-A sub-sag; (**h**) XJ-A sub-sag).

4.2. Major Elements

The major elements of hydrocarbon source rocks in the Zhu 1 Depression both showed strong MnO loss; Al_2O_3, CaO, Fe_2O_3, P_2O_5 and TiO_2 showed weak depletion; SiO_2 in addition of the Wenchang Formation in the Enping sub-sag, and the rest of the sample showed weak enrichment; K_2O was in a weak enrichment-weak depletion state (Figure 4a–e).

Table 3 lists the test information of major element oxides. The samples in this study were mainly composed of SiO_2, Al_2O_3, K_2O, and Fe_2O_3, accounting for about 76.295–96.007% of the total major elements, with 86.1% on average. SiO_2 accounted for 52.136–77.77%, with 65.11% on average; at the same time, Al_2O_3 provided a certain proportion (11.45–23.22%), with 16.71% on average; K_2O (2.417–7.864%, 4.067% on average) and

Fe_2O_3 (0.891–11.579%, average 4.28%) content was almost the same. The relative abundance of other major element oxides was low.

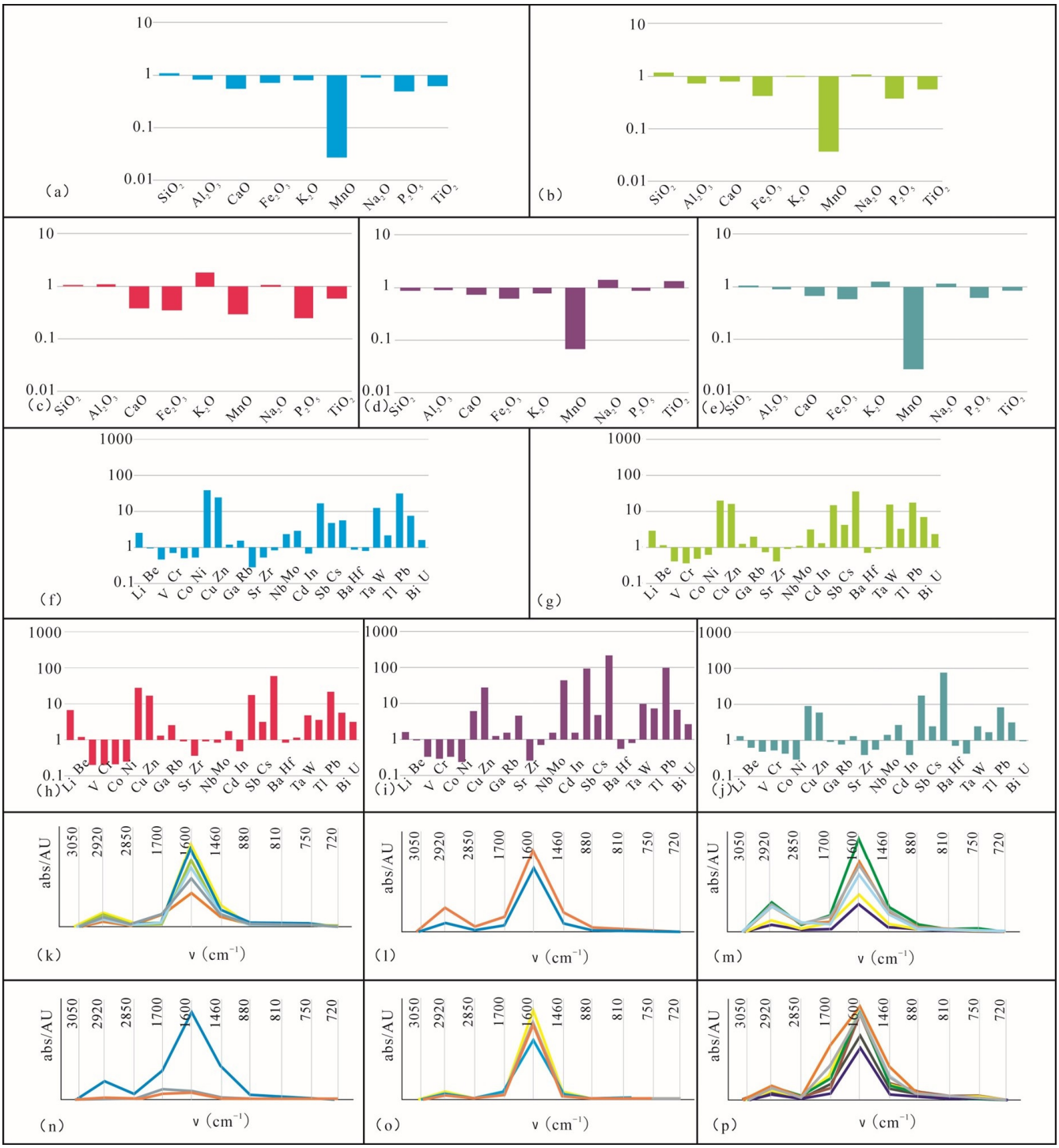


Figure 4. Major and trace element enrichment map and infrared spectrum characteristics of hydrocarbon source rocks in the Zhu-1 Depression. ((**a**), XJ-A sub-sag Enping Formation; (**b**), EP-A sub-sag Enping Formation; (**c**), XJ-A sub-sag Wenchang Formation; (**d**), EP-A sub-sag Wenchang Formation; (**e**), HZ-A sub-sag Wenchang Formation; (**f**), XJ-A sub-sag Enping Formation; (**g**), EP-A sub-sag Enping Formation; (**h**), XJ-A sub-sag Wenchang Formation; (**i**), EP-A sub-sag Wenchang Formation; (**j**), HZ-A sub-sag Wenchang Formation; (**k**) XJ-A-2-1A Enping Formation; (**l**) EP-A-3-1 Enping Formation; (**m**), HZ-A-1-3 Wenchang Formation; (**n**), XJ-A-1-1 Wenchang Formation; (**o**), EP-A-3-1 Wenchang Formation; (**p**), HZ-A-8-1 Wenchang Formation).

Table 3. Major elements data of samples from the hydrocarbon-rich sub-sag of the Zhu-1 Depression.

Sub-Sag	Well Number	Strata	Depth	SiO_2	Al_2O_3	MgO	Na_2O	K_2O	P_2O_5	TiO_2	CaO	Fe_2O_3	MnO	Loss on Ignition	BaO	NiO	Cr_2O_3	CuO	ZrO_2	SrO
			m	%	%	%	%	%	%	%	%	%	%	%	μg/g	μg/g	μg/g	μg/g	μg/g	μg/g
XJ-A	XJ-A-2-1A	1st + 2nd Enping formation	4089.5	62.00	14.93	1.86	1.92	2.81	0.07	0.59	1.92	6.79	0.10	6.54	1991.66	76.14	157.71	329.95	277.11	114.15
			4120.5	69.81	14.39	1.17	1.59	2.72	0.07	0.67	0.95	5.81	0.11	2.64	1576.48	56.86	104.62	55.53	433.32	97.38
			4153.5	66.18	16.02	1.25	1.99	2.86	0.08	0.66	1.08	5.25	0.10	4.50	1557.38	49.97	90.88	37.61	371.65	113.11
			4188.5	68.69	16.05	0.90	1.29	2.75	0.08	0.63	0.42	4.68	0.03	4.44	1202.35	51.58	84.84	27.71	329.48	145.99
			4227.5	72.83	14.37	0.90	1.32	2.55	0.07	0.61	0.45	4.70	0.05	2.14	778.95	51.50	98.22	25.34	469.55	94.98
			4271.5	65.71	16.55	0.86	1.58	2.62	0.07	0.67	0.40	4.44	0.04	7.01	1528.99	50.17	88.91	30.75	336.22	119.48
			4302.5	65.29	16.83	0.95	1.33	2.85	0.07	0.63	0.41	4.18	0.03	7.42	979.86	49.22	86.06	28.75	310.72	126.73
			4333.5	73.17	12.99	0.76	0.94	2.47	0.06	0.55	0.60	3.97	0.01	4.47	457.15	50.82	72.77	19.50	512.56	93.07
			4356.5	67.45	17.38	1.11	1.51	5.00	0.09	0.71	0.88	4.12	0.05	1.47	5135.73	45.88	70.02	28.81	339.29	172.45
			4389.5	66.00	17.31	1.05	1.26	4.17	0.10	0.73	0.75	4.89	0.05	3.60	3851.51	52.94	76.63	29.29	346.12	153.28
		3rd Enping formation	4419.5	67.49	15.11	0.91	0.66	2.69	0.08	0.60	0.45	4.74	0.05	7.20	488.68	52.40	87.82	26.59	383.90	111.89
			4446.5	66.96	16.16	0.97	0.63	2.68	0.08	0.64	0.43	4.77	0.06	6.63	434.43	43.59	80.76	24.14	407.04	140.13
			4480.5	60.52	14.57	1.41	0.69	2.63	0.08	0.63	0.81	11.58	0.19	6.87	872.83	63.72	158.07	76.63	319.02	134.73
			4509.5	66.82	15.46	1.06	0.70	2.71	0.08	0.64	0.52	4.84	0.05	7.11	501.44	52.42	89.86	36.04	403.12	120.69
			4544.5	67.41	16.41	1.01	0.76	2.83	0.07	0.64	0.51	4.88	0.04	5.42	459.41	56.85	96.77	104.63	375.03	112.84
			4572.5	67.37	15.75	1.05	0.68	2.76	0.08	0.64	0.43	5.30	0.05	5.87	459.09	61.36	95.83	59.25	374.79	111.95
			4593.5	66.25	16.85	0.93	0.89	3.08	0.08	0.62	0.44	4.33	0.04	6.39	718.80	58.13	71.38	43.98	329.18	99.67
			4622.5	69.48	13.35	1.08	0.70	2.62	0.07	0.53	1.34	4.59	0.04	6.15	466.07	55.68	62.42	25.86	350.77	105.49
			4655.5	71.15	14.62	0.92	0.69	2.69	0.07	0.62	0.95	4.58	0.03	3.66	520.35	55.87	79.20	22.99	403.89	106.82
			4691.5	67.57	18.46	0.93	0.75	3.10	0.06	0.61	0.63	3.98	0.02	3.83	579.64	49.47	76.26	34.46	316.14	101.39
	XJ-A-1-1	2nd Wenchang formation	4450.5	63.14	17.76	0.96	1.43	5.37	0.06	0.76	0.98	4.00	0.04	4.86	9423.29	28.64	44.94	29.16	420.98	211.34
			4495.5	61.77	23.22	0.81	1.36	6.02	0.05	0.76	0.46	3.35	0.01	1.39	11,016.19	27.48	34.61	24.73	360.66	234.70
			4576.5	62.62	21.07	0.81	1.42	7.24	0.04	0.70	0.64	3.34	/	1.43	8855.60	37.74	45.42	18.24	585.05	200.98
			4626.5	64.41	19.82	0.26	1.00	6.72	0.03	0.35	0.20	0.89	/	5.54	7675.66	47.40	13.67	11.43	280.49	144.34
			4674.5	63.74	19.97	0.43	1.16	7.86	0.03	0.40	0.23	1.27	/	4.15	9114.94	47.29	13.43	13.20	237.15	171.15
EP-A	EP-A-3-1	Enping formation	3511.75	77.77	12.13	0.68	1.20	3.55	0.05	0.42	0.92	2.56	/	0.53	3860.29	101.62	31.07	10.00	201.13	131.96
			3577.75	70.45	14.00	0.86	1.12	3.68	0.06	0.54	1.36	3.26	/	4.56	2827.52	74.80	52.37	22.58	322.41	133.68
			3650.5	73.34	14.45	0.66	1.35	3.85	0.05	0.46	0.83	2.44	/	2.41	3202.31	70.81	35.91	21.11	237.55	132.70
			3715	72.34	13.23	0.81	1.34	3.72	0.05	0.50	1.20	2.64	/	3.75	6174.24	105.53	43.17	16.05	237.19	191.67
			3791.5	64.47	15.26	0.83	1.28	3.67	0.08	0.89	0.82	4.22	0.08	7.32	15,482.16	33.89	58.91	53.20	168.73	288.02
		Wenchang formation	4755.5	57.27	16.33	0.87	1.41	3.28	0.13	1.18	0.84	4.48	0.15	11.60	29,576.42	37.22	47.78	73.20	184.74	686.63
			4775.5	55.31	16.32	0.89	1.52	2.87	0.12	1.47	0.85	3.78	0.10	13.38	41,049.23	49.56	48.98	73.78	213.02	999.17
			4812.5	52.14	17.11	0.94	1.64	2.68	0.15	1.44	1.25	4.37	0.14	14.85	39,937.69	42.48	45.23	91.65	202.94	1003.59
			4816.5	55.59	18.27	0.93	1.74	2.91	0.14	1.24	1.03	4.66	0.16	10.68	31,531.66	39.50	52.22	74.70	197.67	734.83
			4822.5	52.62	16.92	0.93	2.06	2.80	0.15	1.38	1.11	4.78	0.16	13.92	38,433.94	44.72	43.52	85.08	196.25	981.13
			4829.5	54.52	17.70	0.94	1.80	2.94	0.13	1.23	0.69	4.98	0.17	12.23	31,758.01	45.24	42.65	67.14	210.47	782.46

Table 3. *Cont.*

Sub-Sag	Well Number	Strata	Depth	SiO_2	Al_2O_3	MgO	Na_2O	K_2O	P_2O_5	TiO_2	CaO	Fe_2O_3	MnO	Loss on Ignition	BaO	NiO	Cr_2O_3	CuO	ZrO_2	SrO
			m	%	%	%	%	%	%	%	%	%	%	%	μg/g	μg/g	μg/g	μg/g	μg/g	μg/g
HZ-A	HZ-A-1-3	Wenchang formation	3807.5	58.63	20.06	1.06	1.48	4.26	0.08	1.11	0.61	3.82	0.05	7.46	19,672.06	31.41	51.30	37.59	310.64	377.57
			3817.5	62.55	19.34	0.98	1.18	3.56	0.08	1.01	0.67	4.06	0.07	5.44	15,784.89	32.06	55.01	39.80	238.42	346.71
			3825.5	70.85	14.91	0.79	0.87	3.31	0.08	0.89	0.67	4.14	0.06	2.22	16,965.91	29.47	41.86	38.64	157.28	341.89
			3837.5	72.35	14.30	0.70	0.85	3.32	0.06	0.87	0.73	3.52	0.06	2.02	17,054.23	25.89	39.21	36.43	164.10	330.72
			3855.5	67.97	16.24	0.91	0.82	3.82	0.07	0.93	1.29	4.00	0.06	2.53	18,749.29	26.49	43.48	41.41	145.75	375.11
			3867.5	68.62	15.89	0.82	0.86	2.42	0.09	0.85	0.97	4.85	0.08	3.73	12,739.22	26.28	46.49	38.61	155.82	285.76
			3880.5	63.63	19.16	1.14	0.99	3.78	0.09	1.05	1.05	4.39	0.07	3.33	18,763.45	31.59	52.13	43.01	198.85	374.78
			3894.5	63.25	17.93	1.07	1.06	3.42	0.12	1.00	1.34	4.18	0.05	5.37	17,613.24	34.50	49.96	43.24	193.16	342.79
	HZ-A-5-1	5th Wenchang formation	4578.5	54.81	18.31	1.22	1.71	6.42	0.07	1.00	0.80	3.26	0.08	11.12	17,295.56	46.56	64.22	67.13	225.25	350.53
			4589.5	56.55	19.50	1.17	1.70	5.47	0.08	0.95	0.78	3.99	0.10	8.90	12,910.39	46.64	69.00	63.96	226.32	305.07
			4607.5	56.07	18.61	1.09	1.51	4.20	0.11	0.98	0.97	4.82	0.11	10.71	13,500.94	45.60	74.20	56.71	208.48	345.06
			4622.5	59.32	17.44	1.02	1.35	4.76	0.08	0.99	0.71	4.17	0.06	8.85	17,866.36	38.07	69.42	55.06	182.77	343.85
			4637.5	67.63	12.89	0.69	1.16	3.59	0.06	0.82	0.65	4.04	0.05	7.31	15,575.17	33.11	52.57	44.70	135.61	273.49
			4651.5	70.13	11.45	0.63	1.13	4.55	0.05	0.81	0.83	3.45	0.04	5.51	19,258.10	29.95	45.07	43.15	107.94	266.14
			4662.5	63.13	14.61	1.06	1.12	6.53	0.12	0.86	1.39	4.37	0.08	5.38	18,873.32	30.19	49.91	74.03	141.37	257.01
			4676.5	64.01	16.07	0.96	1.17	4.24	0.09	0.91	0.95	4.76	0.06	5.71	15,645.44	32.82	60.05	49.33	166.60	227.88
	HZ-A-8-1	4th Wenchang formation	4422.5	67.63	16.74	1.08	1.29	6.03	0.11	0.72	0.67	3.96	0.02	1.53	5752.65	55.58	68.74	29.48	326.41	179.94
			4440.5	66.85	16.90	1.08	1.28	6.33	0.11	0.75	0.71	3.63	0.03	1.42	9010.32	47.28	69.34	37.49	287.87	231.19
			4454.5	69.88	16.65	1.00	1.65	4.86	0.11	0.78	0.72	3.80	0.02	0.08	7925.21	44.43	69.98	37.44	303.20	207.86
			4460.5	68.11	16.69	1.04	1.53	5.72	0.10	0.72	1.62	3.57	0.04	0.51	6442.71	40.69	64.48	30.74	325.15	191.15
			4468.5	66.65	17.28	1.09	1.70	5.29	0.11	0.72	1.43	3.88	0.03	1.48	6414.27	46.93	68.20	36.60	300.90	196.07
			4477.5	65.75	17.76	1.20	1.56	6.82	0.10	0.76	0.57	3.72	0.03	1.25	8129.92	43.73	72.97	34.81	272.99	216.81
			4493.5	67.49	16.99	1.07	1.31	6.61	0.10	0.71	0.62	3.56	0.03	0.92	7273.90	45.72	68.34	30.28	302.38	199.30
			4507.5	66.79	17.03	1.07	1.59	5.14	0.10	0.73	1.24	3.94	0.04	2.09	5419.08	44.92	73.34	28.56	314.95	179.76
			4522.5	65.65	17.90	1.10	1.71	4.50	0.13	0.78	1.19	4.31	0.03	2.41	6220.20	52.87	77.68	35.63	302.27	197.06
			4539.5	64.10	18.64	1.17	1.94	4.58	0.12	0.77	0.95	4.33	0.04	3.02	6737.89	46.19	76.92	40.78	286.06	203.44
		5th Wenchang formation	4747.5	58.07	21.44	1.54	2.03	5.87	0.16	0.87	0.93	4.48	0.08	3.67	13,309.36	44.45	59.92	62.23	168.35	339.27
			4762.5	64.62	18.78	0.94	1.51	3.81	0.10	0.80	0.63	3.99	0.06	4.09	10,693.17	39.57	65.05	50.33	148.75	263.11
			4777.5	67.67	18.23	0.84	1.39	4.50	0.08	0.81	0.81	3.66	0.04	1.05	13,290.33	33.78	51.58	47.40	129.24	304.96
			4792.5	65.63	19.23	0.85	1.39	3.61	0.10	0.79	0.60	4.00	0.08	3.08	10,488.85	38.42	59.62	47.48	135.58	254.68
			4807.5	55.91	21.19	1.10	1.80	4.00	0.18	0.83	0.63	6.85	0.27	6.63	11,557.92	38.39	61.24	86.90	135.94	300.17
			4822.5	62.16	18.29	1.07	1.58	4.67	0.22	0.83	0.65	5.58	0.11	3.94	14,284.71	35.02	55.61	58.03	130.60	331.53
			4837.5	71.72	13.08	0.72	1.25	3.45	0.07	0.71	0.54	4.71	0.04	2.74	13,486.80	32.12	45.45	54.71	107.82	273.76
			4852.5	71.31	14.45	0.66	1.25	3.38	0.09	0.69	1.17	4.53	0.08	1.68	10,879.56	31.97	47.46	42.98	114.96	251.44
			4865.5	67.59	15.45	0.98	1.45	4.23	0.12	0.77	1.26	4.42	0.05	2.78	13,215.40	34.49	49.06	45.91	137.61	286.58

Legend: "/" means data not detected; "LOI" (loss on ignition); "μg/g" means microgram per gram.

4.3. Trace Elements

Figure 4f,g show that the high-temperature mineralization element W is relatively enriched in the hydrocarbon source rocks of the Enping Formation in the Zhu-1 Depression, and the enrichment factor is between 10 and 100. The enrichment factors of the metal ore-forming elements Cu, Zn, Sb, Pb, Cd, Tl, Bi, and Ga were in the range of enrichment-relatively enriched. The enrichment factors of rock-forming elements Li, Rb, Cs, and Ba and the radioactive elements U were between 1~10. The high-temperature ore-forming elements Nb, Zr, Hf, Ta, iron group elements V, Cr, Ni, and Co, and rock-forming elements Be and Sr showed weak depletion. Figure 4h–j show that the hydrocarbon source rocks of the Wenchang Formation are enriched in metal ore-forming elements Sb, Pb, and Cd, and most of Cu, Zn, Cd, Cd, Tl, and Bi are in the enrichment. The enrichment factor of group Ba element is >100. The rock-forming elements Li, Rb, and Cs, high-temperature ore-forming element W and radioactive element U are enriched. Be, Ga, Hf, and Ta are in weak enrichment-weak depletion. Iron group elements V, Cr, Co, and Ni, the high temperature ore-forming elements Zr, Nb, and Mo and the metal ore-forming element were all depleted (Equation (1)).

Table 4 lists the trace element test information. The top five trace element proportions in the hydrocarbon source rocks of Enping Formation are shown as follows: Ba content 517.57 μg/g~38,039.30 μg/g, average 4876.09 μg/g; and Cu content 26.31 μg/g~5118.51 μg/g, average 1884.49 μg/g; Zn content 174.66 μg/g~3685.70 μg/g, average 1617.78 μg/g; Pb content 81.48 μg/g~3545.21 μg/g, average 352.13 μg/g; Rb content 61.88 μg/g~225.67 μg/g, average 149.26 μg/g. The trace element proportions of hydrocarbon source rocks in Wenchang Formation and Enping Formation are slightly different, with the top five being as follows: Ba content 7543.71 μg/g~112,973.92 μg/g, average 38,950.06 μg/g, Zn content 117.83 μg/g~3342.73 μg/g, average 686.60 μg/g; Rb content 187.99 μg/g~1932.37 μg/g, average 632.00 μg/g; Cu content 42.30 μg/g~3377.58 μg/g, average 577.63 μg/g, and Pb content 63.38 μg/g~1300.61 μg/g, average 267.27 μg/g, accounting for the top five trace elements.

4.4. Infrared Spectrum

Ruan et al. [30] believed that the main absorption band had a definite relationship with its chemical structure. For example, 3600–3200 cm^{-1} was an asymmetric broadband with the maximum absorption around 3400 cm^{-1}. This absorption came from the stretching vibration of OH group from alcohol, phenol, and carboxylic acid. Tarrow band at 3050–3030 cm^{-1} had very weak absorption and stretching vibration of CH on aromatic nucleus, and different absorption bands correspond to different chemical functional groups.

Table 5 lists the Infrared spectrum test information. As shown in the figure (Figure 4k–p), the intensity of the Paleogene kerogen absorption peak at 1600 cm^{-1} is stronger in the study area, indicating that the composition of higher plants, such as lignin and cellulose, contributed a large amount; absorption peaks at 2920, 2850, and 1460 cm^{-1} are also observed, indicating that animals with higher fat content and lower plants (algae) also made certain contributions. The intensities of absorption peaks at 2920, 2850, and 1460 cm^{-1} were generally lower than 1600 cm^{-1}, reflecting the infrared spectrum characteristics of lacustrine mixed kerogen in the area.

Table 4. Trace elements data of samples from the hydrocarbon-rich sub-sag of the Zhu-1 Depression.

Sub-Sag	Well Number	Strata	Depth m	7Li μg/g	9Be μg/g	47Ti μg/g	51V μg/g	52Cr μg/g	59Co μg/g	60Ni μg/g	63Cu μg/g	66Zn μg/g	71Ga μg/g	85Rb μg/g	88Sr μg/g	90Zr μg/g	93Nb μg/g	95Mo μg/g	114Cd μg/g	115In μg/g	121Sb μg/g	133Cs μg/g	137Ba μg/g	178Hf μg/g	181Ta μg/g	184W μg/g	185Re μg/g	205Tl μg/g	208Pb μg/g	209Bi μg/g	238U μg/g
XJ-A	XJ-A-2-1A	1st + 2nd Enping formation	4089.5	59.52	3.27	4191.13	83.17	134.64	20.50	69.35	2488.00	3216.25	19.22	154.78	136.22	105.76	19.01	7.17	0.82	0.12	10.26	17.34	4512.57	3.24	1.96	113.47	0.01	1.03	3545.21	3.05	4.26
			4120.5	44.60	2.72	3807.66	69.14	89.94	14.67	43.01	1125.17	1007.35	17.77	142.99	103.09	116.22	18.82	3.21	0.36	0.08	3.11	14.63	2890.14	3.18	1.80	28.37	0.00	0.98	453.28	1.28	4.24
			4153.5	56.75	3.78	3482.86	70.88	72.54	11.52	33.26	732.27	653.06	18.35	149.09	103.07	90.92	17.51	1.71	0.28	0.09	2.19	17.55	2177.12	2.92	1.54	12.04	0.00	1.08	176.18	1.16	3.98
			4188.5	51.54	2.03	3163.95	60.59	37.43	11.74	25.01	62.67	174.66	17.11	135.60	147.58	82.14	16.94	1.14	0.35	0.06	1.89	16.17	2676.87	2.60	1.42	10.63	0.00	0.88	83.05	0.83	4.10
			4227.5	36.87	1.99	3104.91	54.42	41.20	10.43	28.25	1032.76	817.30	15.99	129.49	88.95	100.30	16.94	2.24	0.35	0.05	2.00	12.78	1532.69	2.93	1.51	12.03	0.00	0.86	134.59	0.85	3.70
			4271.5	48.49	2.53	3413.45	62.57	45.99	11.33	24.91	46.18	190.61	17.52	136.24	97.24	90.86	17.54	1.43	0.41	0.07	1.78	16.15	2566.34	2.93	1.57	10.62	0.00	0.76	81.48	0.82	4.44
			4302.5	58.14	3.74	3350.27	68.60	76.39	12.74	33.62	1250.94	1004.75	18.46	142.97	110.95	88.03	17.17	2.30	0.53	0.07	2.73	16.25	2128.30	2.93	1.59	13.01	0.00	0.94	154.35	1.03	4.78
			4333.5	35.01	2.40	3140.96	50.60	37.04	11.34	27.38	1240.92	1035.99	15.78	122.55	74.26	102.17	16.11	1.14	0.34	0.05	1.95	10.67	573.35	3.08	1.40	10.96	0.00	0.85	117.96	0.78	3.84
			4356.5	39.87	2.53	2957.58	55.71	57.84	10.20	23.88	786.93	648.13	15.61	120.90	208.68	65.33	16.24	1.35	0.45	0.04	2.70	12.18	9826.69	2.13	1.44	13.03	0.00	0.82	105.44	0.76	3.85
			4389.5	44.44	2.55	3161.80	60.50	67.67	10.49	28.07	895.43	743.26	16.98	138.30	217.57	64.35	17.32	2.42	0.46	0.05	2.99	13.43	10,671.40	2.15	1.56	7.12	0.00	0.95	177.96	0.88	4.48
		3rd Enping formation	4419.5	54.58	3.20	3623.07	69.01	77.61	12.49	42.05	2796.82	2061.21	18.74	146.89	91.39	94.69	18.44	2.42	0.68	0.08	3.45	14.77	735.07	3.01	1.67	8.15	0.00	1.20	202.56	1.20	4.29
			4446.5	57.07	2.60	3504.05	60.50	69.41	11.01	42.05	3221.16	2307.90	17.26	134.28	98.40	90.44	17.53	1.75	0.74	0.08	3.23	13.56	781.09	3.00	1.57	6.50	0.00	0.91	203.45	1.81	4.36
			4480.5	56.75	2.60	3087.44	92.51	143.19	15.50	53.11	1859.66	1582.40	17.38	127.50	122.52	87.29	16.39	19.25	0.63	0.08	4.95	15.23	1583.75	2.66	1.53	25.00	0.00	1.19	393.10	1.43	4.53
			4509.5	47.65	2.53	3247.81	60.68	49.83	13.94	45.31	2361.61	1737.75	17.02	130.44	78.92	84.64	16.03	3.45	0.52	0.07	2.88	13.99	645.74	2.69	1.49	13.65	0.00	0.99	170.22	1.10	3.72
			4544.5	47.71	2.98	3168.64	60.77	69.85	15.87	52.76	2863.18	2046.10	16.96	133.39	79.37	78.95	16.22	5.82	0.71	0.09	3.41	13.81	517.57	2.53	1.52	19.04	0.00	0.93	229.14	1.28	3.85
			4572.5	51.96	2.32	3249.38	61.99	48.06	16.43	44.39	2477.43	2138.68	17.37	134.05	81.98	79.60	16.17	4.56	0.54	0.06	3.01	14.56	705.93	2.34	1.47	20.53	0.00	0.91	260.96	1.16	3.66
			4593.5	61.33	2.82	3467.80	63.57	70.88	13.17	49.09	3648.56	3357.59	20.21	159.95	84.63	74.51	19.00	2.69	0.83	0.10	3.43	16.15	1362.26	2.36	1.83	11.49	0.00	1.15	328.62	1.62	6.16
			4622.5	45.88	2.20	2815.37	49.77	40.04	12.03	51.67	5118.51	3685.70	15.29	122.09	80.21	74.96	14.48	1.55	0.83	0.08	3.84	11.11	595.70	2.24	1.57	18.38	0.00	0.97	343.02	1.58	3.43
			4655.5	47.41	2.83	3292.75	58.19	106.82	12.09	49.66	3769.30	2860.17	16.94	130.74	75.21	86.03	16.23	1.77	0.72	0.07	3.27	13.06	554.17	2.38	1.57	9.67	0.00	0.95	271.11	1.39	3.60
			4691.5	68.45	4.16	3565.26	66.73	81.28	12.97	48.35	3897.75	2756.81	20.19	153.62	77.58	75.95	18.87	2.06	0.75	0.06	3.43	14.18	518.15	2.46	1.82	9.17	0.00	1.12	275.10	1.46	5.59
	XJ-A-1-1	2nd Wenchang formation	4450.5	55.56	3.67	2475.74	40.88	36.92	8.32	18.44	1135.08	884.34	17.76	198.28	394.96	58.35	16.87	1.44	0.38	0.05	3.08	9.61	28,029.23	2.31	1.71	5.16	0.00	1.73	265.39	0.88	6.60
			4495.5	70.10	2.95	2133.90	34.47	18.57	6.02	11.63	565.08	475.21	18.93	203.09	508.47	44.54	17.09	0.97	0.19	0.05	3.84	6.63	35,189.47	1.75	1.96	5.83	0.00	1.37	262.27	0.88	7.62
			4576.5	79.43	3.49	2525.32	33.52	18.59	6.44	10.76	479.49	403.18	22.26	214.91	302.32	80.47	21.39	1.18	0.32	0.05	2.87	10.28	19,324.62	2.96	1.84	6.84	0.00	1.35	179.05	0.44	6.37
			4626.5	191.41	2.63	1002.99	12.24	13.70	2.53	27.42	3377.58	2469.61	17.31	225.10	279.88	62.21	17.13	1.75	0.53	0.05	3.93	8.86	19,538.10	2.88	2.83	9.13	0.00	1.51	358.74	1.34	10.06
			4674.5	261.70	3.51	1136.16	14.67	14.61	2.66	25.28	1963.77	1459.35	18.80	307.44	342.32	54.32	18.57	1.12	0.35	0.05	3.35	11.23	24,226.91	2.56	3.17	9.09	0.00	2.00	294.68	1.28	11.95
EP-A	EP-A-3-1	Enping formation	3511.75	66.94	3.46	2955.94	47.86	23.73	11.08	79.98	3290.23	2654.33	20.02	211.25	242.17	60.76	20.66	1.55	0.88	0.13	3.95	12.47	10,544.04	1.99	2.26	34.34	0.00	1.58	389.22	1.68	8.26
			3577.75	55.88	2.85	2922.10	51.52	29.71	11.56	39.09	1379.15	1142.04	18.17	188.74	150.79	74.17	17.96	1.29	0.46	0.18	2.37	16.58	4951.43	2.37	1.74	25.19	0.00	1.52	201.80	1.20	5.55
			3650.5	70.04	4.03	3071.86	50.41	26.93	11.83	28.84	39.32	614.59	20.75	225.67	197.03	67.47	21.26	0.82	0.38	0.14	1.91	16.36	7721.85	2.02	2.20	20.41	0.00	1.60	132.24	1.26	7.77
			3715	61.77	3.02	2922.17	47.63	46.21	11.11	63.93	26.31	389.99	19.55	210.78	287.11	56.20	21.93	0.92	0.43	0.12	2.76	12.16	13,090.99	2.07	2.24	31.84	0.00	1.59	180.61	1.15	7.44
			3791.5	27.50	2.16	2856.94	78.13	55.67	14.95	26.96	702.08	827.69	15.80	61.88	502.24	82.20	10.30	3.22	0.93	0.07	3.72	4.54	38,039.30	2.18	0.78	4.91	0.00	0.90	192.71	0.55	2.80
		Wenchang formation	4755.5	34.30	2.86	2266.34	52.02	43.98	8.97	20.07	543.28	3342.73	17.74	134.12	1472.17	50.07	13.83	2.80	8.27	0.16	16.81	14.71	97,633.39	2.02	1.53	12.28	0.00	3.05	1262.23	1.10	6.58
			4775.5	36.65	2.52	2189.02	45.55	31.86	8.46	18.61	45.89	1324.88	18.41	152.44	1425.83	62.84	14.56	2.00	6.80	0.13	16.03	16.09	92,450.57	2.02	1.65	16.04	0.00	3.20	1075.36	1.13	7.74
			4812.5	30.63	3.04	2090.39	43.26	30.09	7.89	16.22	42.31	1206.70	18.52	138.30	1758.21	50.49	14.62	2.14	7.94	0.13	19.82	14.63	112,973.93	1.99	1.63	13.40	0.00	3.64	1292.12	1.10	7.39
			4816.5	31.59	2.94	2024.22	43.16	24.94	7.83	16.44	270.13	1794.51	18.03	131.02	1675.56	31.47	14.62	2.35	9.25	0.17	18.28	13.60	72,285.23	1.38	1.59	12.98	0.00	3.32	1223.51	1.10	6.28
			4822.5	26.03	2.40	1902.42	39.79	26.00	8.12	20.11	520.30	1665.80	18.20	132.40	1932.37	29.77	13.90	2.28	10.58	0.12	20.16	11.82	89,662.88	1.27	1.53	14.36	0.00	3.27	1300.61	1.08	6.82
			4829.5	31.16	2.31	2269.42	44.56	23.07	8.32	17.71	589.11	2158.58	20.04	144.52	1800.01	36.80	15.28	2.01	9.04	0.18	19.40	12.44	89,297.23	1.37	1.61	18.38	0.00	3.15	1217.90	1.18	7.18

Table 4. *Cont.*

Sub-Sag	Well Number	Strata	Depth m	7Li μg/g	9Be μg/g	47Ti μg/g	51V μg/g	52Cr μg/g	59Co μg/g	60Ni μg/g	63Cu μg/g	66Zn μg/g	71Ga μg/g	85Rb μg/g	88Sr μg/g	90Zr μg/g	93Nb μg/g	95Mo μg/g	114Cd μg/g	115In μg/g	121Sb μg/g	133Cs μg/g	137Ba μg/g	178Hf μg/g	181Ta μg/g	184W μg/g	185Re μg/g	205Tl μg/g	208Pb μg/g	209Bi μg/g	238U μg/g
HZ-A	HZ-A-1-3	Wenchang formation	3807.5	19.49	1.24	2895.91	58.67	32.06	9.09	20.35	782.35	705.32	17.29	83.62	673.38	85.16	12.71	1.05	0.77	0.05	4.22	6.83	52,709.55	2.76	1.00	3.70	0.00	0.87	204.21	0.43	2.83
			3817.5	17.92	0.67	2327.78	56.07	26.56	8.67	18.31	464.17	410.74	13.84	62.45	849.74	84.46	9.22	1.42	1.30	0.04	3.80	5.90	55,885.54	2.43	0.70	3.61	0.00	0.93	151.91	0.44	2.65
			3825.5	17.01	1.29	2161.99	56.32	33.34	8.95	17.66	480.31	411.15	12.75	52.93	675.40	65.81	8.01	1.48	0.53	0.03	3.63	5.41	48,515.07	2.17	0.60	4.29	0.00	0.89	143.36	0.37	2.20
			3837.5	16.86	1.43	1892.05	51.19	29.60	7.32	16.05	552.91	454.20	11.81	54.59	686.40	53.38	7.18	1.52	0.43	0.03	3.41	4.20	49,513.43	1.67	0.55	3.44	0.00	0.91	145.91	0.31	1.88
			3855.5	19.63	0.89	2172.80	64.16	27.94	9.54	17.15	475.80	411.76	13.51	53.59	764.24	59.59	7.32	1.71	0.64	0.04	3.75	5.38	54,322.38	2.03	0.55	3.81	0.00	1.02	154.81	0.38	2.09
			3867.5	25.22	1.06	2553.16	63.60	30.19	10.40	19.92	738.90	587.94	15.00	57.26	672.67	73.40	8.62	1.50	0.50	0.04	4.08	6.09	45,295.40	2.34	0.64	3.76	0.00	0.70	143.59	0.45	2.20
			3880.5	22.52	1.61	2713.66	64.21	30.40	10.85	20.61	543.76	467.17	16.31	61.08	797.19	80.90	9.25	1.41	0.50	0.04	4.14	7.05	51,396.29	2.64	0.69	4.07	0.00	0.75	143.20	0.97	2.34
			3894.5	20.04	0.90	2235.80	53.64	30.05	9.66	18.28	363.92	340.56	13.05	54.01	844.33	72.21	7.74	1.15	0.64	0.05	4.27	6.16	55,914.59	2.31	0.58	3.67	0.00	0.87	149.19	0.34	1.95
	HZ-A-5-1	5th Wenchang formation	4578.5	19.97	1.55	3183.77	70.24	38.92	22.70	26.13	500.21	419.11	16.27	52.65	391.47	81.20	9.49	1.47	0.41	0.04	2.71	3.18	25,823.46	2.41	0.62	2.39	0.00	0.98	101.75	0.39	2.24
			4589.5	24.19	1.26	3800.38	84.33	48.52	24.00	30.27	602.51	483.98	19.96	58.88	361.14	98.62	11.04	1.64	0.44	0.05	2.43	3.90	20,432.92	2.83	0.71	2.54	0.00	0.74	99.97	0.44	2.64
			4607.5	29.24	1.45	3858.87	93.27	57.36	17.56	33.10	883.52	719.05	19.89	61.83	458.61	84.27	12.28	3.15	0.45	0.06	3.05	4.61	25,751.29	2.56	0.81	3.11	0.00	0.78	119.46	0.51	2.76
			4622.5	24.36	2.41	2910.75	82.82	53.62	12.14	27.05	583.26	461.00	16.93	58.22	533.91	80.86	10.70	3.48	0.35	0.04	3.96	5.09	40,233.46	2.62	0.74	3.53	0.00	0.87	113.05	0.45	3.19
			4637.5	17.52	1.06	2155.80	75.13	53.84	9.93	21.97	436.48	368.24	12.58	47.62	564.51	59.59	7.95	4.93	0.33	0.04	4.19	3.64	48,646.01	1.93	0.52	3.93	0.00	0.84	106.41	0.34	2.41
			4651.5	17.01	1.62	1774.47	65.36	50.98	9.22	20.94	632.58	496.89	10.99	42.31	598.80	48.34	7.47	4.54	0.41	0.04	4.82	2.99	54,757.42	1.54	0.46	3.26	0.00	0.74	130.64	0.36	1.85
			4662.5	19.63	1.55	2237.33	73.80	55.09	10.52	20.58	525.18	419.75	12.02	45.23	458.35	71.50	7.49	4.16	0.33	0.03	4.26	3.80	40,364.07	2.23	0.52	3.44	0.00	0.69	101.68	0.33	2.11
			4676.5	17.57	0.87	2391.17	79.19	66.92	11.36	23.38	394.07	351.15	13.77	55.44	542.26	88.64	9.03	3.12	0.38	0.05	4.36	6.22	49,995.83	2.82	0.63	4.08	0.00	0.71	102.64	0.38	2.69
	HZ-A-8-1	4th Wenchang formation	4422.5	33.73	2.37	2848.50	54.47	64.70	9.81	21.90	332.12	303.31	14.35	108.93	211.23	62.00	16.20	1.02	0.66	0.04	2.71	13.63	9044.49	2.16	1.32	4.08	0.00	0.79	66.46	0.77	3.42
			4440.5	35.15	1.97	2916.41	52.49	64.63	9.20	21.81	407.95	342.70	13.26	100.50	260.62	65.98	14.81	0.99	0.41	0.05	2.98	11.93	11,894.21	2.13	1.25	4.18	0.00	0.71	70.33	0.71	3.19
			4454.5	28.83	2.72	2610.37	47.82	59.42	8.40	20.18	430.18	357.29	12.35	94.52	251.85	54.87	13.59	0.88	0.39	0.05	2.69	11.08	11,299.31	2.20	1.26	3.65	0.00	0.68	68.79	0.64	3.00
			4460.5	33.21	1.63	2908.65	52.07	66.25	9.03	23.44	720.16	546.81	13.73	100.44	187.99	55.42	14.95	0.88	0.48	0.04	2.66	12.22	7543.72	1.92	1.29	3.69	0.00	0.71	82.41	0.69	3.19
			4468.5	32.58	2.21	2816.59	52.28	43.18	9.17	21.87	577.54	464.46	13.45	98.04	203.77	59.47	14.17	0.86	0.48	0.03	2.58	11.87	8387.12	2.00	1.20	3.62	0.00	0.70	75.72	0.65	3.18
			4477.5	40.45	3.51	3190.43	61.28	78.68	10.04	24.82	557.20	452.57	15.30	114.00	232.95	64.94	16.60	1.13	0.51	0.05	3.00	14.80	9745.63	2.15	1.38	4.31	0.00	0.80	83.68	0.80	3.56
			4493.5	32.53	1.93	2935.91	54.62	92.22	9.08	24.75	541.80	430.17	14.41	108.84	209.38	78.13	15.59	0.96	0.53	0.03	2.91	13.29	8473.07	2.38	1.37	4.08	0.00	0.76	77.96	0.76	3.86
			4507.5	38.32	2.22	3302.68	60.05	121.29	10.18	27.73	464.30	391.84	15.06	111.62	200.80	71.24	16.58	0.95	0.47	0.05	2.62	13.60	8085.52	2.05	1.43	4.11	0.00	0.77	69.31	0.69	3.58
			4522.5	39.67	2.15	3167.64	61.71	73.14	10.33	26.82	617.13	503.66	15.46	111.26	253.24	61.86	15.95	0.99	0.63	0.05	2.88	13.92	11,212.26	1.99	1.36	4.05	0.00	0.79	80.90	0.99	3.45
			4539.5	36.93	2.47	2813.45	58.14	63.19	10.17	24.12	358.58	317.97	14.48	101.74	237.82	63.07	13.50	0.96	0.52	0.04	2.57	12.94	10,268.86	1.82	1.11	3.55	0.00	0.73	65.82	0.69	3.57
		5th Wenchang formation	4747.5	31.68	2.09	2601.98	62.53	60.95	10.98	22.88	57.29	117.83	15.48	63.74	629.60	60.74	10.97	1.41	0.74	0.04	3.10	6.24	34,130.03	2.06	0.77	3.16	0.00	0.49	63.38	0.50	3.09
			4762.5	23.60	1.73	2553.79	69.13	67.71	10.64	24.09	302.88	302.35	15.67	57.22	572.55	66.42	10.99	2.21	0.47	0.05	3.13	5.16	30,616.58	2.05	0.76	2.93	0.00	0.50	73.84	0.52	3.46
			4777.5	23.67	2.08	2396.35	67.62	47.34	9.78	19.52	258.93	257.87	13.85	51.64	579.20	48.62	10.28	2.11	0.66	0.04	3.32	4.75	32,725.92	1.74	0.69	2.95	0.00	0.50	71.18	0.50	2.75
			4792.5	22.99	1.94	2502.50	73.05	47.50	11.58	23.88	429.84	366.22	14.79	54.26	430.33	46.84	11.04	2.93	0.42	0.05	2.90	4.67	30,250.47	1.68	0.71	3.16	0.00	0.56	80.55	0.58	1.99
			4807.5	22.80	2.94	2645.83	76.54	47.95	12.67	23.58	370.65	333.28	15.83	61.52	531.24	53.68	12.62	3.03	0.48	0.05	3.42	5.04	35,097.94	1.69	0.83	3.46	0.00	0.64	83.58	0.55	2.41
			4822.5	22.22	2.16	2428.93	79.68	53.51	11.57	22.90	331.43	316.23	15.30	60.32	654.78	58.54	11.11	3.15	0.57	0.04	3.64	5.77	35,611.29	2.17	0.76	4.18	0.00	0.63	86.92	0.45	3.05
			4837.5	20.87	1.69	1900.00	68.80	40.54	8.39	18.67	339.91	285.55	10.99	52.87	575.41	37.10	9.78	5.20	0.50	0.03	3.96	4.72	34,867.84	1.33	0.57	4.11	0.00	0.78	87.06	0.34	1.69
			4852.5	25.13	1.33	2445.76	74.56	43.01	9.46	21.39	586.03	445.05	12.85	50.52	493.50	48.90	10.38	3.66	0.38	0.04	3.60	5.11	29,281.12	1.63	0.64	3.96	0.00	0.53	86.28	0.44	1.75
			4865.5	17.08	0.74	2015.21	58.79	43.30	8.82	19.42	395.07	355.56	12.07	51.76	591.42	56.74	8.89	3.37	0.33	0.03	5.30	6.73	32,999.14	1.91	0.60	3.57	0.00	0.52	76.77	0.32	2.10

Legend: "7Li" 7 means relative atomic mass and Li means chemical elements; "μg/g" means microgram per gram.

Table 5. Infrared spectrum data of samples from the hydrocarbon-rich sub-sag of the Zhu-1 Depression.

Sub-Sag	Well Number	Strata	Depth m	Abs/AU 3050	2920	2850	1700	1600	1460	880	810	750	720
XJ-A	XJ-A-2-1A	1st + 2nd Enping formation	4188.50	0	7.541	1.44	3.135	59.48	10.36	1.11	1.8	0.83	0
			4356.50	0	4.866	0.858	11.28	33.53	9.427	1.98	1.06	1.11	0
			4389.50	0	8.64	1.067	11.93	48.49	12.25	2.48	1.44	1.37	0
		3rd Enping formation	4572.50	0	13.83	3.891	3.308	82.2	21.22	1.96	2.23	1.19	0
			4593.50	0	8.465	2.075	3.997	79.73	16.55	3.19	2.73	2.24	0
			4655.50	0	12.4	1.665	2.771	66.84	11.9	2.14	2.17	1.67	0
	XJ-A-1-1	2nd Wenchang formation	4450.50	0	10.92	3.363	17.83	53.82	19.83	3.01	1.77	1.16	0
			4626.50	0	0.85	0.196	3.584	4.422	0.955	0	0	0	0
			4674.50	0	0.867	0.196	6.125	5.166	1.493	0	0	0	0
EP-A	EP-A-3-1	1st + 2nd Enping formation	3577.75	0	0.833	0.165	0.611	6.335	0.832	0.11	0.18	0.05	0
			3791.50	0	2.338	0.51	1.488	8.017	1.836	0.4	0.33	0.21	0
		3rd Enping formation	4755.50	0	0.643	0.139	0.575	4.806	0.563	0.1	0.14	0.05	0
			4775.50	0	0.378	0.053	0.47	6.145	0.317	0.08	0.08	0.04	0
			4812.50	0	0.375	0.059	0.504	6.302	0.465	0.07	0.11	0.03	0
			4822.50	0	0.677	0.106	0.555	7.212	0.606	0.03	0.1	0.04	0
HZ-A	HZ-A-1-3	4th Wenchang formation	3825.50	0	5.825	1.632	1.656	11.5	3.484	0.53	0.26	0.11	0
			3880.50	0	5.014	1.465	2.044	14.06	4.123	0.86	0.35	0.15	0
			3894.50	0	5.655	1.52	3.068	13.29	4.308	0.63	0.33	0.28	0
	HZ-A-5-1	5th Wenchang formation	4578.50	0	2.235	0.515	1.751	7.471	1.612	0.47	0.18	0.13	0
			4607.50	0	1.47	0.39	0.646	6.067	0.965	0.41	0.19	0.17	0
			4637.50	0	5.928	1.368	3.229	18.63	4.982	1.5	0.65	0.76	0
	HZ-A-8-1	4th Wenchang formation	4422.50	0	1.416	0.208	4.043	11.23	2.915	0.69	0.2	0.22	0
			4440.50	0	1.586	0.26	6.767	11.38	3.956	0.63	0.16	0.42	0
			4493.50	0	1.046	0.212	4.331	9.566	2.715	0.54	0.15	0.32	0
			4507.50	0	1.04	0.207	3.113	11.01	1.844	0.52	0.18	0.4	0
			4522.50	0	0.886	0.169	2.639	9.702	1.672	0.41	0.14	0.13	0
		5th Wenchang formation	4762.50	0	1.495	0.341	2.6	10.72	1.795	0.83	0.37	0.4	0
			4792.50	0	0.664	0.15	0.82	6.413	0.636	0.33	0.2	0.15	0
			4822.50	0	1.428	0.233	1.454	10.53	1.982	0.95	0.46	0.48	0
			4852.50	0	0.922	0.164	1.866	7.925	1.252	0.59	0.32	0.37	0

Legend: "/" means data not detected; "abs/AU" means absorbance unit.

4.5. Microcomponents

The classification of organic microscopic components in hydrocarbon source rocks should adhere closely to the principles of origin as outlined by Teichmüller [31]. Palynologists employ transmitted light to categorize kerogen into five groups: amorphous, algae, herbaceous, woody, and coal. Petrologists utilize reflected light and fluorescence to divide kerogen into three groups: exinite, vitrinite, and inertinite. Nowadays, whole rock analysis methods have gradually developed, mainly combining reflected light and fluorescence, to directly identify and statistically analyze the microscopic components of source rock samples, obtain the relative percentage content data of each microscopic component in the whole rock, and thus distinguish the type of organic matter in source rocks. In this study, kerogen was categorized into four components: sapropelite, exinite, vitrinite, and inertinite. Sapropelite encompasses sapropel amorphous bodies, alginite, and sapropel clastic bodies; exinite comprises resinite, sporinite, suberinite, cutinite, fungal spores, exinitic clastic bodies, and humus amorphous bodies; vitrinite includes structural vitrinite and unstructured vitrinite; finally, inertinite refers to fusinite. Please refer to Table 6 for specific values.

In Paleogene hydrocarbon source rocks, the order of prevalence for organic components is as follows: sapropelite > exinite ≈ inertinite > vitrinite. The hydrocarbon source rocks of the Wenchang Formation exhibit a relatively high content of sapropelite + exinite (ranging from 56.6% to 68.6%, with an average of 62.5%). Conversely, the content of sapropelite + exinite in the hydrocarbon source rocks of the Enping Formation displays significant variation (ranging from 35.6% to 67.3%, with an average of 59%), with the

content of sapropelite lower than that of the Wenchang Formation, accompanied by a higher presence of inertinite.

The hydrocarbon source rocks of the Wenchang Formation demonstrate robust hydrocarbon generation potential, yielding crude oil and wet gas + condensate oil products. In contrast, the hydrocarbon source rocks of the Enping Formation exhibit average hydrocarbon potential, yielding wet gas + condensate oil products (Figure 5).

Table 6. Microscopic components of source rock data of samples from the hydrocarbon-rich sub-sag of the Zhu-1 Depression.

Sub-Sag	Well Number	Strata	Depth m	Sapropelinite	Exinite	Vitrinite	Inertinite
XJ-A	XJ-A-2-1A	1st + 2nd Enping formation	4188.50	93	66	159	86
			4356.50	116	85	201	70
			4389.50	121	81	26	72
		3rd Enping formation	4572.50	133	66	199	71
			4593.50	126	76	202	70
			4655.50	130	66	196	78
	XJ-A-1-1	2nd Wenchang formation	4450.50	92	78	55	75
			4626.50	139	65	204	56
			4674.50	125	74	199	65
EP-A	EP-A-3-1	1st + 2nd Enping formation	3577.75	70	37	93	100
			3791.50	80	70	150	100
		3rd Enping formation	4755.50	135	53	37	75
			4775.50	130	74	204	66
			4812.50	132	74	206	77
			4822.50	122	79	201	72
HZ-A	HZ-A-1-3	4th Wenchang formation	3825.50	110	81	30	79
			3880.50	130	54	184	80
			3894.50	126	66	192	76
	HZ-A-5-1	5th Wenchang formation	4578.50	120	60	180	90
			4607.50	106	74	35	85
			4637.50	95	70	45	90
	HZ-A-8-1	4th Wenchang formation	4422.50	107	63	170	80
			4440.50	113	83	196	66
			4493.50	110	70	40	80
			4507.50	102	71	51	76
			4522.50	110	64	56	70
		5th Wenchang formation	4762.50	127	64	38	71
			4792.50	125	71	196	75
			4822.50	120	70	190	80
			4852.50	130	60	190	78

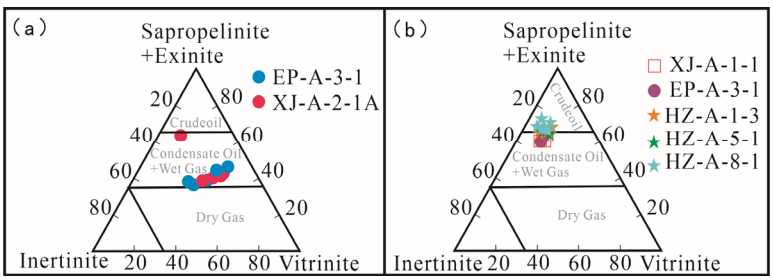


Figure 5. Microscopic composition of Paleogene hydrocarbon source rocks in the Zhu-1 Depression. ((**a**), Enping Formation; (**b**) Wenchang Formation).

5. Discussion

5.1. Paleoenvironment

5.1.1. Paleoclimate

The degree of chemical weathering serves as a valuable indicator of past climate variations, offering insights into paleoclimate changes. Researchers have identified various geochemical indicators, such as Sr and Cu contents, as well as ratios like Sr/Cu, Mg/Ca, FeO/MnO, Al_2O_3/MgO, and SiO_2/Al_2O_3, which are commonly used to assess paleoclimate environments. However, it is important to consider factors such as the size of the lake basin, water depth, and presence of free water surfaces, as these can lead to differences in ion concentrations and overall precipitation amounts. To reconstruct paleoclimate conditions, several geochemical proxies have been developed, including the chemical index of alteration (CIA), chemical index of weathering (CIW), and plagioclase index of alteration (PIA). The CIA, introduced by Nesbitt and Young in 1982, has been widely applied to estimate the paleoclimate of mud rocks (lutites) due to its minimal interference factors.

In this study, the chemical index of alteration (CIA) and C index were utilized to analyze the chemical weathering history using molecular ratios. These indices offer valuable insights into the intensity of chemical weathering processes over time, aiding in the reconstruction of past climate conditions.

$$\mathrm{CIA} = \mathrm{mole}\,[\mathrm{Al_2O_3}/(\mathrm{Al_2O_3} + \mathrm{CaO^*} + \mathrm{Na_2O} + \mathrm{K_2O})] \times 100 \quad (2)$$

$$\mathrm{CaO^*} = \mathrm{moleCaO} - \mathrm{moleP_2O_5} \times 10/3 \quad (3)$$

$$\mathrm{C} = \frac{\sum(\mathrm{Fe} + \mathrm{Mn} + \mathrm{Cr} + \mathrm{V} + \mathrm{Ni} + \mathrm{Co})}{\sum(\mathrm{Ca} + \mathrm{Mg} + \mathrm{Sr} + \mathrm{Ba} + \mathrm{K} + \mathrm{Na})} \quad (4)$$

The interpretation of chemical weathering indices such as the Chemical Index of Alteration (CIA) and the C index provides valuable insights into past climatic conditions. Generally, high CIA values (80–100) suggest intense chemical weathering in hot and humid climates, intermediate values (70–80) correspond to warm and humid climates, while low values (50–70) indicate weaker weathering under cold and arid climates [32]. Similarly, the C index offers additional information: values below 0.4 indicate arid climates as the predominant background, values above 0.6 suggest mostly sub-humid environments, and values between 0.4 and 0.6 represent transitional climates.

Palynological studies [33] have indicated that Paleogene climate variations in South China generally aligned with global trends. Early Eocene climates were characterized by hotter and arid conditions, while temperatures cooled, and humidity increased from the Middle Eocene to Oligocene. The rise in humidity was influenced by the uplift of the Qinghai-Tibet Plateau and the development of the East Asian monsoon. The Paleogene climate in the Zhu-1 Depression mirrored that of South China during the same period.

Comparing the CIA values of the Enping Formation to those of the Wenchang Formation (Figure 6a), along with the C values (Figure 6b), it is observed that the Enping Formation exhibits slightly higher CIA (Equations (2) and (3)) and C values (Equation (4)). Consequently, the climatic backdrop during the Wenchang period is inferred to have been warmer and drier, whereas the Enping period experienced cooler and wetter conditions in the study area.

5.1.2. Paleo-Salinity

Paleo-salinity serves as a crucial indicator in paleoenvironmental analysis, aiding in the reconstruction of paleogeography and paleoclimate during sedimentary periods. Lake water salinity predominantly influences the influx and evaporation rates of external waters, exerting significant control over the types of organisms and sediments within lakes.

In lake environments, the migration ability of Sr exceeds that of Ba. Consequently, as water salinity increases and mineralization rises, Ba precipitates first in the form of $BaSO_4$, followed by the gradual enrichment and precipitation of Sr within the water body [34]. Studies by Berner et al. [35] on sediments in waters with varying salinities revealed that the ratio of sulfur (S) to total organic carbon (TOC) could accurately reflect sedimentary water salinity, with a positive correlation and a slope of approximately 2.8:1 for the TOC:S ratio. However, in lake systems with low sulfate concentrations, such as most lake environments, other oxidants (or the organic matter itself) typically serve as the primary electron acceptors, resulting in generally low S values and little to no relationship between S and TOC (Figure 6c).

The typical hydrocarbon source rocks of the Enping Formation predominantly formed in waters with low salinity, representing freshwater lake basin sediments. Wells Wen 4 and Wen V exhibited salinity characteristics, suggesting freshwater-brackish water environments (Figure 6d). These findings may indicate more separate and independent paleogeographical patterns during the Wenchang period. However, it is noteworthy that paleo-salinity levels between different wells exhibited some degree of fluctuation.

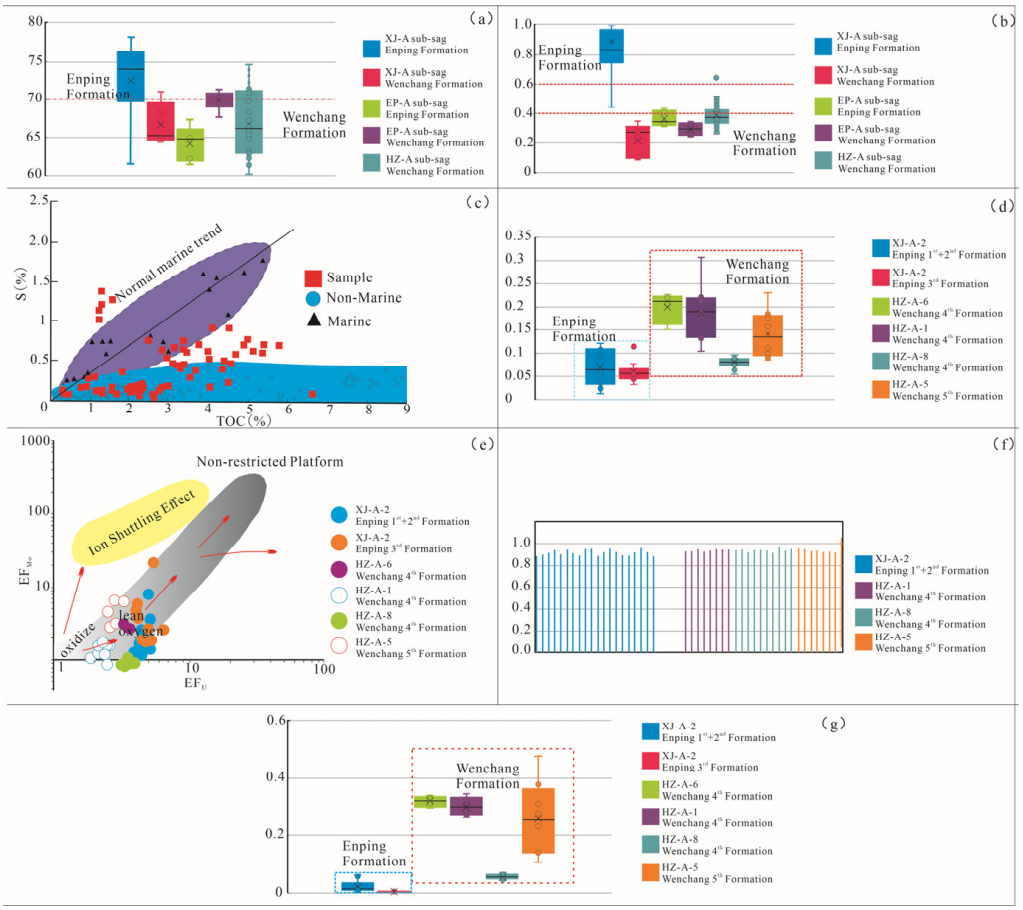


Figure 6. Paleoenvironment characteristics of hydrocarbon source rocks in the Zhu-1 Depression. ((**a**), CIA values (Equations (2) and (3)) for hydrocarbon source rocks in the Zhu-1 Depression; (**b**), C value (Equation (4)) for hydrocarbon source rocks in the Zhu-1 Depression; (**c**), paleo-salinity map of hydrocarbon source rocks in the Zhu-1 Depression (Berner et al. (1984) [35]); (**d**), distribution of S/TOC values for hydrocarbon source rocks in the Zhu-1 Depression; (**e**), Mo-U (Equation (1)) covariation model of hydrocarbon source rocks in the Zhu-1 Depression; (**f**), Statistical diagram of cerium anomaly (δCe) in the hydrocarbon source rocks of the Zhu-1 Depression; (**g**), Ba/Al diagram of hydrocarbon source rocks in the Zhu-1 Depression).

5.1.3. Paleo-Redox

The EF-Mo and EF-U co-variation models proposed by Algeo and tribovillard [25] are widely used in paleo-environment reconstruction [36,37]. This is due to the difference in the geochemical behavior of U and Mo. In oxygenated seawater, U exists in the form of U(VI), and Mo exists in the form of Mo(VI), mainly in the form of molybdate (MoO_4^{2-}). In an oxygen environment, MoO_4^{2-} is mainly co-precipitated in the form of ferromanganese shell and manganese nodules or adsorbed on manganese-oxyhydroxide [38,39]. Under deoxygenated conditions close to the Fe(III)-Fe(II) transformation, soluble U(VI) is reduced to insoluble U(IV), and the presence of organic substrates can accelerate this process [40]. Under this situation, self-generated U (U_{auth}) was preferentially enriched in the sediments of authigenic Mo (Mo_{auth}). In an anoxic environment, in the presence of a small amount of dissolved hydrogen sulfide, MoO_4^{2-} is converted to a series of particle-reactive thiomolybdate ions ($MoS_{4-x}O_x^{2-}$) [41]. If there is a large amount of free H_2S, under this condition, the enrichment rate of Moauth far exceeds that of Uauth, resulting in a gradual increase in the (Mo/U) content in the sediments [25]. In addition, Mo uptake in sediments may be influenced by the Fe–Mn cycle as thiomolybdates react with particulates and easily adsorbed by Mn-Fe-oxyhydroxides [42]. Mn-Fe-oxyhydroxides form in the overlying water column (under oxic-suboxic conditions) and adsorbed thiomolybdates when they pass through the chemocline. Then, Mn-Fe-oxyhydroxides dissolve in the underlying water column (under more intensely reducing conditions) and release Mo, which is scavenged by sulfurized OM or Fe–S phases [42]. Thus, Mo accumulation can be accelerated through Mn-Fe-oxyhydroxide shuttling within the water column.

As shown in the figure (Figure 6e), the hydrocarbon source rocks in the Zhu-1 Depression were not affected by the ion shuttling effect; the EF-U (Equation (1)) and EF-Mo (Equation (1)) of the samples were positively correlated, suggesting that most hydrocarbon source rocks were formed in the oxygen-poor bottom water environment, indicating that the sedimentary bottom water had oxygen intrusion to a certain extent, which may be related to the strong terrestrial input of the lake basin during the sedimentation period.

Rare earth elements (REEs) typically exhibit a positive trivalence in nature. However, cerium (Ce) possesses a unique property in that it can also exist in a positive tetravalence state, setting it apart from other REEs. This dual valence behavior of Ce distinguishes it from other trivalent REEs and leads to anomalous behavior when it lacks its normal positive trivalence [43]. In sedimentary environments, different conditions can lead to positive or negative anomalies in REEs. Consequently, the δCe anomaly is commonly used as an indicator to assess the oxidation-reduction state of the sedimentary environment. A δCe value less than 1 indicates a deficit, signifying an oxidizing environment, while a δCe value greater than 1 suggests normal or excess concentrations, indicating a reducing environment. The rare-earth element test information provided in Table 7 reveals that δCe values were consistent with the results of Mo-U analysis (Figure 6f), with most values hovering around 1.0. This characterization aligns with a transitional environment between weakly oxidizing and weakly reducing conditions. The δCe anomaly thus serves as a valuable tool for understanding the redox conditions of sedimentary environments and provides insights into the geochemical processes occurring within these settings.

Table 7. Rare earth element data of samples from the hydrocarbon-rich sub-sag of the Zhu-1 Depression.

Sub-Sag	Well Number	Strata	Depth m	45Sc μg/g	89Y μg/g	139La μg/g	140Ce μg/g	141Pr μg/g	146Nd μg/g	147Sm μg/g	153Eu μg/g	157Gd μg/g	159Tb μg/g	163Dy μg/g	165Ho μg/g	166Er μg/g	169Tm μg/g	172Yb μg/g	175Lu μg/g	232Th μg/g
XJ-A	XJ-A-2-1A	1st + 2nd Enping formation	4089.5	10.93	23.48	45.73	85.50	10.30	36.77	6.88	1.83	6.11	0.97	4.84	0.93	2.54	0.41	2.29	0.37	22.78
			4120.5	10.07	26.35	46.07	86.46	10.36	36.82	6.81	1.57	6.16	0.96	5.12	0.90	2.60	0.41	2.92	0.38	22.97
			4153.5	11.25	25.79	44.81	86.80	10.21	36.18	6.81	1.52	6.10	0.95	4.77	0.97	2.63	0.42	2.55	0.38	22.43
			4188.5	9.66	23.03	41.67	82.85	9.39	33.76	6.31	1.47	6.31	1.16	4.81	0.87	2.96	0.51	2.21	0.35	19.63
			4227.5	9.12	21.94	45.07	86.19	10.40	36.27	6.65	1.28	5.85	0.90	4.55	0.87	2.38	0.42	2.34	0.34	21.07
			4271.5	10.56	22.11	44.52	87.63	9.96	35.24	6.46	1.49	5.91	0.95	4.59	0.91	2.53	0.39	2.47	0.38	21.84
			4302.5	10.58	24.71	48.76	93.34	11.01	39.02	7.20	1.50	6.48	1.01	5.59	1.13	2.83	0.43	3.12	0.38	23.18
			4333.5	8.19	21.88	50.27	93.44	11.38	41.06	7.20	1.15	6.32	0.97	4.62	0.86	2.29	0.38	2.23	0.33	24.08
			4356.5	8.54	18.49	37.82	76.13	8.69	31.25	5.92	2.40	5.25	0.83	3.94	0.80	2.40	0.33	1.86	0.29	18.37
			4389.5	9.60	25.85	40.77	81.56	9.18	32.56	6.51	2.68	5.84	0.90	4.25	0.82	2.20	0.34	2.02	0.31	20.36
		3rd Enping formation	4419.5	10.78	25.57	53.35	100.07	12.30	43.38	7.97	1.36	7.25	1.10	5.14	0.98	2.69	0.44	2.36	0.36	24.05
			4446.5	10.06	23.39	48.09	93.21	10.89	39.33	7.37	1.31	6.57	1.02	6.12	1.01	2.43	0.39	2.17	0.34	21.27
			4480.5	9.92	21.80	44.36	89.01	10.08	36.11	6.60	1.32	6.00	0.97	4.43	0.86	3.11	0.38	2.82	0.34	20.37
			4509.5	9.59	23.76	45.94	88.48	10.29	36.23	6.59	1.20	5.93	0.94	4.50	0.87	2.34	0.37	2.24	0.33	19.94
			4544.5	9.48	25.91	48.89	91.94	11.15	39.42	7.26	1.22	6.59	1.02	5.56	0.88	2.89	0.40	2.24	0.35	21.98
			4572.5	9.89	22.53	45.89	85.64	10.28	36.46	6.81	1.21	5.97	1.07	4.34	0.83	3.35	0.36	2.10	0.34	20.23
			4593.5	10.70	38.37	58.32	112.69	13.12	46.12	8.58	1.46	7.91	1.23	6.05	1.16	3.17	0.50	2.79	0.44	25.80
			4622.5	8.44	22.22	42.93	86.80	9.85	35.14	6.63	1.17	6.02	1.12	5.28	1.04	2.28	0.37	2.11	0.30	18.43
			4655.5	9.67	22.57	45.50	88.17	10.34	36.49	6.65	1.13	5.94	0.97	4.31	0.82	2.21	0.39	2.85	0.31	19.22
			4691.5	10.92	26.47	51.94	97.20	12.08	41.07	7.78	1.26	6.93	1.10	5.99	0.97	2.63	0.54	2.40	0.36	23.52
	XJ-A-1-1	2nd Wenchang formation	4450.5	7.98	24.08	43.34	83.24	9.83	34.67	6.69	4.81	6.12	1.24	4.78	0.96	2.62	0.41	2.44	0.37	29.45
			4495.5	7.33	20.35	48.05	89.38	10.40	35.45	6.69	5.96	6.06	0.97	5.31	0.91	2.56	0.40	3.60	0.36	29.86
			4576.5	7.90	23.68	65.47	123.23	14.52	48.91	8.64	3.95	7.75	1.19	5.58	1.06	2.81	0.45	2.60	0.40	30.47
			4626.5	3.39	23.69	32.22	64.03	7.23	24.65	4.94	3.28	5.07	1.06	4.04	0.85	2.51	0.44	2.55	0.41	37.74
			4674.5	3.71	17.19	30.40	59.40	6.98	23.35	4.87	4.00	4.53	0.99	3.61	0.91	2.90	0.38	2.37	0.34	39.87
EP-A	EP-A-3-1	Enping formation	3511.75	8.69	22.38	49.76	91.39	10.88	37.40	6.96	2.62	6.32	1.05	5.32	0.94	2.57	0.40	2.51	0.37	28.58
			3577.75	8.84	23.55	46.91	88.07	10.31	35.24	6.81	1.79	6.05	0.97	7.97	0.86	2.35	0.37	2.76	0.33	24.20
			3650.5	9.59	23.77	47.47	89.04	10.41	35.27	6.95	2.16	6.20	0.99	4.77	0.94	2.68	0.40	2.59	0.37	31.62
			3715	9.14	22.92	44.41	86.41	9.70	33.49	8.07	2.94	5.92	0.95	4.53	0.88	2.48	0.39	2.17	0.34	27.93
			3791.5	10.23	16.98	32.41	67.60	7.40	26.82	5.29	6.57	4.97	0.76	3.67	0.72	2.21	0.33	1.89	0.29	10.73
		Wenchang formation	4755.5	8.87	21.16	46.26	92.04	10.44	36.94	7.86	16.06	7.49	1.08	6.14	0.97	2.65	0.42	2.46	0.69	22.43
			4775.5	8.33	23.07	50.27	97.70	11.00	38.62	8.32	15.56	7.58	1.08	5.30	1.04	2.62	0.42	3.71	0.42	24.40
			4812.5	8.06	26.73	52.93	97.99	11.83	41.48	8.68	18.58	8.19	1.14	6.66	1.06	2.89	0.47	2.78	0.46	25.93
			4816.5	7.79	20.03	46.52	88.35	10.44	36.39	8.07	12.57	7.28	1.02	4.54	0.89	2.48	0.38	2.17	0.34	23.82
			4822.5	7.56	22.40	48.54	88.76	10.62	37.17	7.76	14.23	7.07	1.02	4.79	0.88	2.50	0.39	2.31	0.35	23.99
			4829.5	8.33	23.50	52.41	94.61	11.49	40.37	8.50	14.37	7.80	1.33	5.26	1.02	2.70	0.42	2.49	0.37	27.35

Table 7. *Cont.*

Sub-Sag	Well Number	Strata	Depth m	45Sc μg/g	89Y μg/g	139La μg/g	140Ce μg/g	141Pr μg/g	146Nd μg/g	147Sm μg/g	153Eu μg/g	157Gd μg/g	159Tb μg/g	163Dy μg/g	165Ho μg/g	166Er μg/g	169Tm μg/g	172Yb μg/g	175Lu μg/g	232Th μg/g
HZ-A	HZ-A-1-3	Wenchang formation	3807.5	10.55	19.95	42.02	80.57	9.15	32.23	6.30	8.83	5.69	0.92	4.35	0.87	2.39	0.37	2.29	0.36	12.94
			3817.5	8.80	16.59	31.60	61.23	6.94	24.61	4.93	9.18	4.57	0.71	3.56	0.72	2.04	0.32	2.01	0.31	9.72
			3825.5	9.37	16.41	27.83	55.48	6.31	22.39	4.59	7.99	4.37	0.67	3.36	0.70	1.95	0.31	1.93	0.31	8.54
			3837.5	7.70	12.80	24.98	47.85	5.41	19.15	3.86	7.84	3.53	0.54	2.67	0.53	1.51	0.24	1.52	0.24	7.63
			3855.5	10.83	16.70	27.08	53.10	6.14	22.18	4.57	8.91	4.36	0.68	3.50	0.71	2.03	0.54	1.92	0.31	8.45
			3867.5	12.02	18.83	30.78	61.45	7.03	25.60	5.16	7.89	5.02	0.78	4.04	1.07	2.27	0.37	2.19	0.35	9.72
			3880.5	11.96	19.58	33.45	66.72	7.57	27.19	5.46	8.85	5.15	0.82	4.18	0.84	2.37	0.37	2.35	0.36	10.42
			3894.5	9.69	17.80	28.92	59.38	6.73	24.35	5.07	9.64	4.96	0.76	3.86	0.79	2.19	0.35	2.15	0.33	9.09
	HZ-A-5-1	5th Wenchang formation	4578.5	10.83	18.09	37.55	75.90	8.66	31.11	5.91	5.11	5.32	0.83	3.99	0.78	2.23	0.33	2.09	0.32	8.56
			4589.5	12.27	22.40	42.00	84.31	9.66	34.70	6.20	4.30	5.63	0.89	4.59	0.94	2.54	0.41	2.49	0.38	9.91
			4607.5	13.16	21.14	39.02	76.98	9.01	32.57	6.04	4.93	5.38	0.87	4.43	0.90	2.56	0.40	2.30	0.37	10.66
			4622.5	11.29	18.35	32.13	62.96	7.24	26.11	5.26	6.81	4.90	0.77	4.03	0.79	2.26	0.36	2.19	0.34	10.54
			4637.5	8.65	14.26	23.52	45.54	5.24	18.72	3.86	7.56	3.56	0.55	2.96	0.60	1.82	0.29	1.70	0.27	7.56
			4651.5	7.12	11.96	19.16	36.99	4.20	15.14	3.25	8.39	3.10	0.46	2.46	0.49	1.41	0.22	1.39	0.23	6.63
			4662.5	9.58	18.47	21.97	42.40	4.89	17.79	3.65	6.48	3.69	0.59	2.98	0.61	1.85	0.28	1.84	0.27	7.22
			4676.5	10.91	19.21	28.05	59.45	6.39	23.71	4.96	8.06	4.72	0.77	4.01	0.81	2.28	0.36	2.31	0.34	9.48
	HZ-A-8-1	4th Wenchang formation	4422.5	8.77	18.85	36.59	72.96	8.40	29.63	5.99	2.33	5.11	0.81	3.87	0.75	2.04	0.35	2.18	0.29	16.44
			4440.5	9.00	17.20	35.23	70.48	8.03	27.92	5.52	2.67	4.84	0.75	4.17	0.70	1.93	0.30	2.97	0.28	15.66
			4454.5	7.71	16.62	32.75	64.05	7.51	26.69	5.31	2.61	4.41	0.78	3.55	0.67	2.53	0.30	1.93	0.27	15.00
			4460.5	9.42	18.64	35.17	69.80	7.95	28.11	5.29	2.04	4.67	0.76	3.54	1.18	1.91	0.30	2.83	0.29	15.24
			4468.5	8.63	16.65	34.37	68.59	7.93	28.03	5.33	2.19	4.56	0.73	3.46	0.81	2.35	0.32	1.90	0.28	13.77
			4477.5	10.33	19.62	37.85	74.96	8.56	30.50	5.93	2.43	5.07	0.81	3.74	0.76	2.14	0.33	2.11	0.31	15.76
			4493.5	9.29	18.80	35.42	70.37	8.51	28.80	5.96	2.25	5.15	0.79	3.90	0.76	2.09	0.63	2.30	0.29	16.13
			4507.5	9.89	18.55	36.82	74.30	8.23	29.27	5.57	2.08	4.82	0.76	4.19	0.69	1.94	0.34	2.10	0.28	16.11
			4522.5	9.90	18.12	34.82	68.79	7.86	27.55	5.52	2.44	4.77	0.74	3.50	0.69	1.93	0.32	1.98	0.30	15.72
			4539.5	9.59	17.35	32.72	66.19	7.56	26.86	5.32	2.34	4.58	0.74	3.48	0.68	1.94	0.31	2.88	0.29	14.40
		5th Wenchang formation	4747.5	10.59	20.78	35.43	71.99	8.01	28.44	5.71	6.14	5.28	0.83	4.05	0.84	2.27	0.37	2.45	0.37	12.39
			4762.5	10.54	22.64	36.73	73.90	8.17	28.75	5.85	5.66	5.28	0.84	4.23	0.85	2.41	0.42	2.66	0.38	13.26
			4777.5	8.47	17.26	28.38	56.40	6.34	22.46	4.64	5.77	4.17	0.67	3.43	0.66	1.97	0.31	2.07	0.30	9.56
			4792.5	4.79	15.72	22.93	46.03	5.03	17.83	3.81	5.15	3.46	0.57	2.91	0.58	2.37	0.27	1.78	0.30	6.67
			4807.5	4.45	18.08	26.75	51.13	5.61	19.94	4.18	5.85	4.02	0.66	3.38	0.68	1.87	0.31	2.05	0.32	7.75
			4822.5	10.93	23.31	36.16	70.74	8.02	28.79	5.79	6.42	5.37	0.86	6.19	0.91	2.56	0.43	2.81	0.41	11.23
			4837.5	4.95	10.47	17.52	33.22	3.76	13.40	2.75	5.61	2.48	0.40	1.92	0.40	1.11	0.19	1.27	0.19	5.19
			4852.5	6.36	14.19	19.62	38.56	4.40	15.89	3.42	4.92	3.15	0.51	2.66	0.53	1.49	0.25	1.66	0.25	6.35
			4865.5	8.50	17.17	24.95	49.38	5.66	20.65	4.28	5.58	3.89	0.65	3.35	0.67	1.89	0.31	1.95	0.30	7.95

Legend: "45Sc" 45 means relative atomic mass and Sc means chemical elements; "μg/g" means microgram per gram.

5.1.4. Paleo-Productivity

Organisms have a fixed energy rate in the energy cycle, that is, the amount of organic matter produced per unit time and unit area ($g/(m^2 \cdot a)$) [44]. The productivity mainly includes primary productivity and secondary productivity. The productivity of modern lakes can be measured directly [45]. The productivity measurement of ancient lakes is much more complicated and generally includes the carbon isotope method [46], organic method [47], and paleontological method [48]. A warm and humid climate is favorable for biological development and thus enhances primary productivity, while an arid and cool climate decreases productivity [49,50].

Cu, Ni, and Zn are recognized to exhibit a linear and positive correlation with organic carbon content [51,52]. Elevated levels of Cu, Ni, and Zn typically indicate a high input of organic carbon [53]. These elements are actively released and recycled within waters and sediments. However, it is essential to note that low concentrations of Cu, Ni, and Zn do not necessarily imply low organic carbon input or biological productivity [45].

Ba has long been utilized to study paleo-productivity due to its prolonged storage in water and high preservation efficiency. Scholars evaluate paleo-productivity qualitatively and quantitatively, with higher Ba values generally indicating higher paleo-productivity levels [54]. However, it is crucial to distinguish between biogenic and terrestrial sources of Ba to accurately assess paleo-productivity. Aluminum (Al), as a component of aluminosilicate minerals and a major constituent of the Earth's crust, is employed to determine the content of terrestrial Ba, thereby obtaining the biogenic Ba content [55,56].

The paleo-productivity of typical hydrocarbon source rock samples during the Wenchang period (Wen 4/Wen 5) generally exceeded that observed during the sedimentary period of the Enping Formation (Figure 6g). This suggests that organisms in the lake basin thrived more abundantly during the Wenchang Formation's sedimentary period, likely influenced by the prevailing climate conditions. The paleo-productivity during the Wenchang period exhibited significant fluctuations across a broad range, whereas the Enping period demonstrated relatively stable levels of productivity. This stability during the Enping period may be attributed to the stronger segmentation of the lake basin during the Wenchang period, where external factors could have had a more pronounced impact on paleo-productivity levels.

5.2. Organic Matter Enrichment Conditions

The degree of enrichment of organic matter is controlled by various factors such as paleoclimate, redox environment, paleo-productivity, etc. [57]. The development of lacustrine hydrocarbon sources is closely related to factors such as changes in the accommodating space during the formation of lake basins, the physical and chemical properties of ancient lakes, the sources of nutrients from ancient productivity, and the periodic changes in climate [58]. Alkaline enclosed basins with deep water and moderate salinity are conducive to the development of source rocks; Climate and lake stratification play a certain controlling role in the process of organic matter accumulation; The high paleo-productivity and reduced preservation environment are important factors for the enrichment of organic matter in source rocks [59]. The changes in sedimentary rhythm are directly controlled by the changes in physical, chemical, and biological elements of the water bodies inside the lake basin caused by ancient climate changes. Therefore, studying the development mechanism and controlling factors of source rocks in a specific region is of great significance for understanding the development conditions and quality of source rocks, as well as predicting potential high-quality source rocks.

The principal controlling factors influencing Total Organic Carbon (TOC) enrichment in typical hydrocarbon source rocks of the Enping Formation can be outlined as follows:

ancient oxygen levels exert a significant influence on TOC accumulation, while paleoclimate indirectly affects TOC enrichment (Figure 7). On the other hand, the main controlling factors contributing to TOC enrichment in typical hydrocarbon source rocks of the Wenchang Formation are primarily driven by the impact of paleo-productivity. Additionally, the paleo-oxygen facies represents a significant controlling factor. In contrast, the influences of other paleoenvironmental parameters appear to be relatively obscure. This complexity could be attributed to the more localized and segmented environment of the Wenchang sub-sag, which renders it more susceptible to external influences, resulting in intricate relationships among various factors.

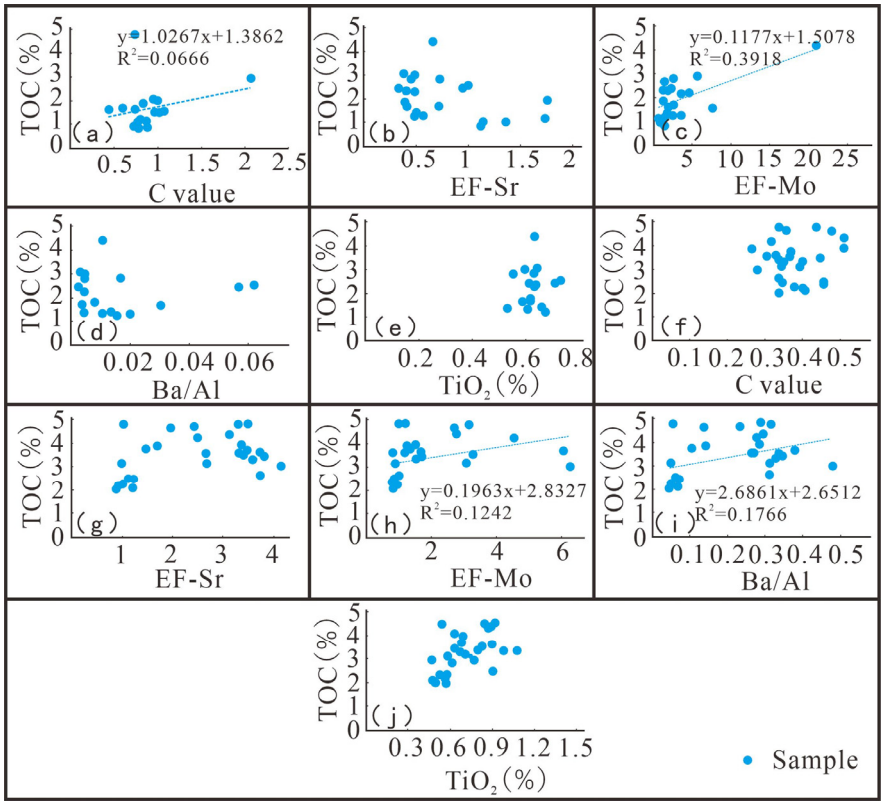


Figure 7. Diagram of the factors controlling the enrichment of organic matter in hydrocarbon source rocks in the Zhu-1 Depression. ((**a**), TOC and C value (Equation (4)); (**b**), TOC and EF-Sr (Equation (1)); (**c**), TOC and EF-Mo (Equation (1)); (**d**), TOC and Ba/AL; (**e**), TOC and TiO_2; (**f**), TOC and C value (Equation (4)); (**g**), TOC and EF-Sr (Equation (1)); (**h**), TOC and EF-Mo (Equation (1)), (**i**), TOC and Ba/AL; (**j**), TOC and TiO_2) ((**a**–**e**) of the Enping Formation; (**f**–**j**) of the Wenchang formation).

Therefore, the most important factor controlling the enrichment of organic matter in the Zhu-1 Depression is the redox environment of the sedimentary waters. The abundance and ratio of trace elements in the sediments can reconstruct the paleo-sedimentary conditions, especially the redox conditions; however, the trace elements will be under the influence of terrestrial components, it is not accurate to simply use the absolute contents of trace elements to determine the redox conditions of a water body. Therefore, although there is some controversy [3,49], V. Ni belongs to the iron group elements, and its ions often exhibit different ionic valence states under different redox conditions. Previous studies have shown that V is prone to combine with sediment to form precipitates in an oxidizing environment, while Ni is prone to adsorption and enrichment under reducing conditions, leading to precipitation. The chemical properties of Th and U elements are very similar in reducing environments but differ greatly under oxidizing conditions. U is tetravalent in a strong reducing state, insoluble in water, and easily enriched. In an oxidized state, it exhibits a

positive hexavalent and is easily soluble in water. Jones et al. [60] summarized a series of discriminant indicators through the study of paleo oxygen facies in a large number of Late Jurassic dark mudstones in Northwest Europe. Through comprehensive comparison, they believed that V/Cr, V/(V + Ni), Ni/Co, and U, and U/Th ratios were the most reliable parameters. They also summarized a set of trace element ratio discriminant indicators for distinguishing the redox environment of bottom water bodies during sediment deposition

The Mo-U covariation model and δCe revealed that the Zhu-1 Depression was in a transitional environment between the oxygen-poor bottom water and weak oxidization-weak reduction. The value of V/(V + Ni) is a good indicator of the redox environment of the Enping Formation and Wenchang Formation in the Zhu-1 Depression, with the ratio falling well between 0.6~0.84, which Hatch and Leventhal [61] considered that oxygen-poor, transitional environment; and V/(V + Ni) and the change in TOC were always positively correlated (the coefficients R^2 of the Enping Formation and the Wenchang Formation were 0.1936 and 0.2605, respectively); V/Cr = 4.25 was not reliable as a boundary between oxygen-poor and anoxic, while V/Cr = 2 was the most reliable as the boundary between oxidation and oxygen-poor. In addition, when V/Cr < 1.2, the DOP values of most of the corresponding data points were less than 0.42, that is, when V/Cr < 1.2, it reflects the oxidized water environment; when greater than 1.2, the environment is poor in oxygen to anoxic [60]. The ratio of V/Cr reached the threshold of oxidation and oxygen-depletion of 2, respectively. However, most oxygen-poor to anoxic environments were >1.2. TOC showed a weak negative correlation in the Enping Formation and a weak negative correlation in the Wenchang Formation, indicating that the V/Cr ratio has an important impact on TOC. The value of Ni/Co was only represented as an anoxic and reducing environment in a few samples, while the rest of the values were represented as oxygen-enriched and oxidizing environment with a relatively low ratio of less than 5.0, and the ratio is relatively low, which indicates that the Ni/Co ratio of this sample is not a good indicator of the redox environment in the Zhu-1 Depression. At the same time, the hydrocarbon source rocks of the Enping and Wenchang Formation in the Zhu-1 Depression had a negative correlation with the Ni/Co value (Figure 8).

V. Ni belongs to the iron group element, and its ions often exhibit different ion valence states under different oxidation-reduction conditions. In oxidized water, V mainly exists in pentavalent forms, such as HVO_4^{2-} and H_2VO_{4-} [62], showing a relatively conservative form. In deep-sea and semi oceanic sediments, V is closely related to the redox cycle of Mn (manganese), and it can adsorb on the hydroxides of Mn and Fe (iron) as well as kaolinite [63,64]. In a mildly reducing environment, V in the pentavalent state is reduced to the tetravalent state, forming VO^{2-} ions, thereby promoting the interaction between hydroxyl containing $VO(OH)_3^-$ and insoluble hydroxide $VO(OH)_2$. When humic acid and fulvic acid are present, this process becomes more significant. Although V cannot form stable sulfides with hydrogen sulfide, its adsorption on organic matter particles is significantly enhanced when hydrogen sulfide appears in pore water. This is because pentavalent V is reduced to tetravalent V ions, which have strong adsorption capacity for organic particles or organic encapsulated particles. In marine environments, the aggregation of V in sediments is mainly achieved through surface adsorption processes or the formation of organometallic complexes [65]. Under strong reduction conditions (such as sulfidation), free H_2S will further reduce V to trivalent state. At this time, trivalent V may be captured by geological porphyrins or precipitated in the form of solid oxide V_2O_3 and hydroxide $V(OH)_3$ [66]. In general, the reduction in V to tetravalent and trivalent states under reducing conditions corresponds to non-sulfurized and sulfurized reduction states, respectively, and V often does not bind with iron sulfides, but precipitates and preserves in the pore water under the reduction zone of iron and manganese hydroxides. Therefore, the degree of enrichment of

V can be used as an indicator parameter of the redox state of water bodies, and the more enriched V is, the more reduced the sedimentary environment is.

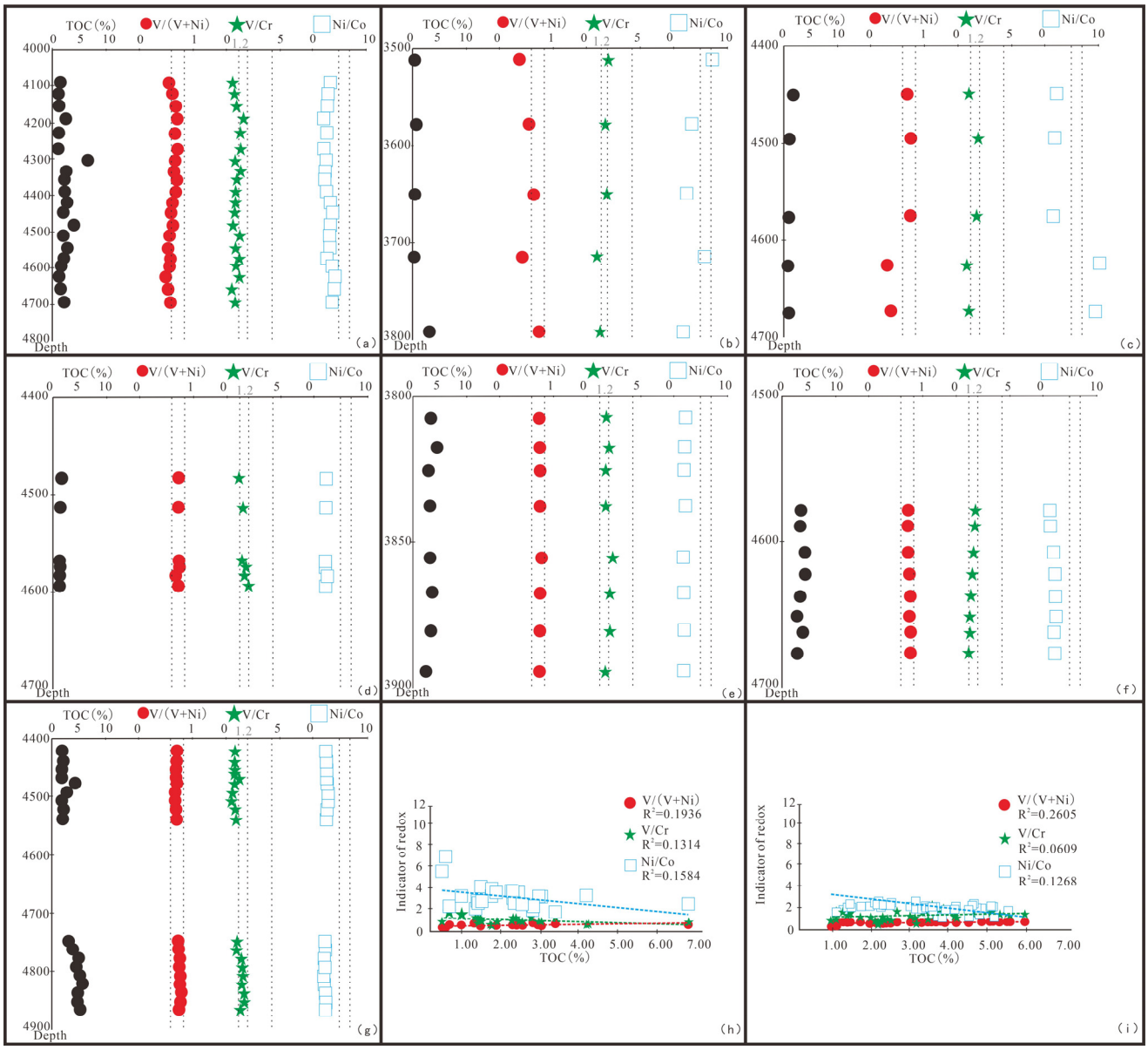


Figure 8. Changes in hydrocarbon source rocks TOC and redox conditions and Relationship between TOC and redox environment for in the Zhu-1 Depression. ((**a**), Enping Formation in the XJ-A-2-1A; (**b**), Enping Formation in the EP-A-3-1; (**c**), Wenchang Formation in the XJ-A-1-1; (**d**), Wenchang Formation in the EP-A-3-1 sub-sag; (**e**), Wenchang Formation in the HZ-A-1-3; (**f**), Wenchang Formation in the HZ-A-5-1; (**g**), Wenchang Formation in the HZ-A-8-1; (**h**), Enping Formation; (**i**), Wenchang Formation). The dashed line is the fitting line for the relationship between TOC and redox environment indicators.

Cr mostly exists in the form of hexavalent chromate anion CrO_4^{2-} in oxidized seawater, and a small portion exists in the form of trivalent pale green $Cr(H_2O)_4(OH)^{2+}$, which is a conservative solubility ion [67]. In the reducing environment, chromate CrO_4^{2-} is reduced to trivalent Cr^{3+} ions and hydroxide ions ($Cr(OH)_2^+$, $Cr(OH)_3$, (Cr, Fe) $(OH)_3$), which form complex compounds with humic acid/fulvic acid or adsorb onto iron hydroxides and manganese hydroxides to precipitate. Therefore, high Cr content generally reflects the reducing environment. It is worth noting that trivalent chromium is rarely captured by self-generated iron sulfides due to its incompatibility with the structure and electrons of

pyrite [68]. Therefore, in the process of bacterial sulfate reduction mineralization of organic matter, Cr does not accumulate in the sediment in the form of sulfides and is subsequently released back into the overlying water through diffusion and horizontal migration during sediment compaction. Moreover, Cr can precipitate into sediments along with terrestrial detrital components such as chromite, clay minerals, and iron magnesium minerals that can replace Mg with Cr [69,70].

Ni mostly exists in the form of dissolved nickel carbonate ($NiCO_3$) in oxidized seawater and can also be adsorbed on humic acid and fulvic acid as Ni^{2+} ions [71]. The formation of complexes between Ni and organic matter accelerates the efficiency of Ni removal from water, leading to Ni enrichment in sediments [72]. As organic matter degrades, Ni will be released into the pore water. In weak reducing environments, due to the lack of Ni ions that can adhere to sulfides and Mn oxides, Ni will re-enter the overlying water. Both Co and Ni are sulfur-loving elements that are soluble in water under oxidative conditions. However, Co can form insoluble CoS and store in sediments under hypoxic conditions, while Ni only forms insoluble NiS under strong reducing conditions [73]. Co may be greatly affected by terrestrial inputs, and therefore the Ni/Co ratio is more influenced by sediment sources and terrestrial inputs. In areas with strong terrestrial inputs, the Co content may increase, leading to a decrease in the Ni/Co ratio and weakening the correlation between Ni/Co and TOC. Ni is easily captured by pyrite in the early diagenetic stage [74], while Co may be released into pore water due to the reduction in Mn oxides, resulting in the masking of the original redox signal.

The adsorption capacity of organic matter for V is significantly higher than that of Ni and Co. The oxygen-containing functional groups (such as -OH, -COOH) in humus preferentially complex with V^{4+} to form stable organic–metal complexes; Ni and Co exist more in the form of free ions or sulfides, and their enrichment is not directly proportional to the abundance of organic matter. The content of oxidation-reduction sensitive trace element V in sediments or sedimentary rocks is controlled by the oxidation-reduction state of the sedimentary environment, and their single source and difficult migration after burial are ideal indicators for paleoenvironmental reconstruction. They have been successfully applied in the reconstruction of paleo-oceanic oxidation-reduction environments [75].

5.3. Composition of Kerogen

Under the influence of temperature and pressure, aliphatic hydrocarbons undergo detachment from the kerogen matrix and predominantly convert into liquid hydrocarbons, serving as the primary source of oil and gas. Functional groups like oxygen generally transform into gaseous byproducts such as CO_2 and H_2O. However, aromatic hydrocarbon structures undergo conversion into semi-char, characterized by fused-ring aromatic configurations with a higher degree of polymerization and aromatization. These structures lack any significant hydrocarbon potential [76]. Kerogen constitutes the primary component of dispersed organic microcomponents within oil shale. It manifests as a complex organic polymer with a three-dimensional amorphous heterogeneous structure, characterized by sheet-like fused aromatic cores connected by aliphatic chains, ether bonds, ester bonds, hydrogen bonds, and π bonds with side chains [77]. Due to their distinct chemical compositions, different types of kerogen exhibit varying abilities to generate oil and gas [78]. Consequently, studying the structure of aliphatic hydrocarbons necessitates an examination of the oil and gas generation potential of kerogen.

Using $(A_{2850} + A_{2920})/\sum A$ as a parameter of fatness, $A_{2850}/(A_{2918} + A_{2850})$ as a parameter of branching degree, $A_{1600}/\sum A$ as a parameter of aromaticity [79], controlled by the influence of higher plant input during the sedimentation period, the aroma parameters of the Enping Formation were mostly higher than those of the Wenchang Formation, while

the Wenchang Formation had an advantage in terms of fatness and branching parameters (Figure 8a–f). The parameters of the three types of functional groups in the Wenchang Formation and the Enping Formation are complex and influenced by maturity and sedimentary environment. As shown in Figure 9j–l, maturity controls the change in the kerogen functional group structure under different sedimentary environments. With the increase in maturity, the fatness parameters and branching parameters of hydrocarbon source rocks of different sedimentary facies showed a decreasing trend (semi-deep lacustrine facies changes are more pronounced), while the aromaticity parameter has steadily increased. During the hydrocarbon formation process of the hydrocarbon source rocks, the CH long chain of the aliphatic alkane structure gradually breaks, hydrocarbons are continuously formed and released, and the proportion of relatively stable C=C aromatics structure gradually increased. At the same time, the functional group proportions of hydrocarbon source rocks formed under different sedimentary environments were different: from delta → shallow lake → semi-deep lake, the fatness parameter gradually increased, while the aromaticity parameter decreased significantly (Figure 9g–i).

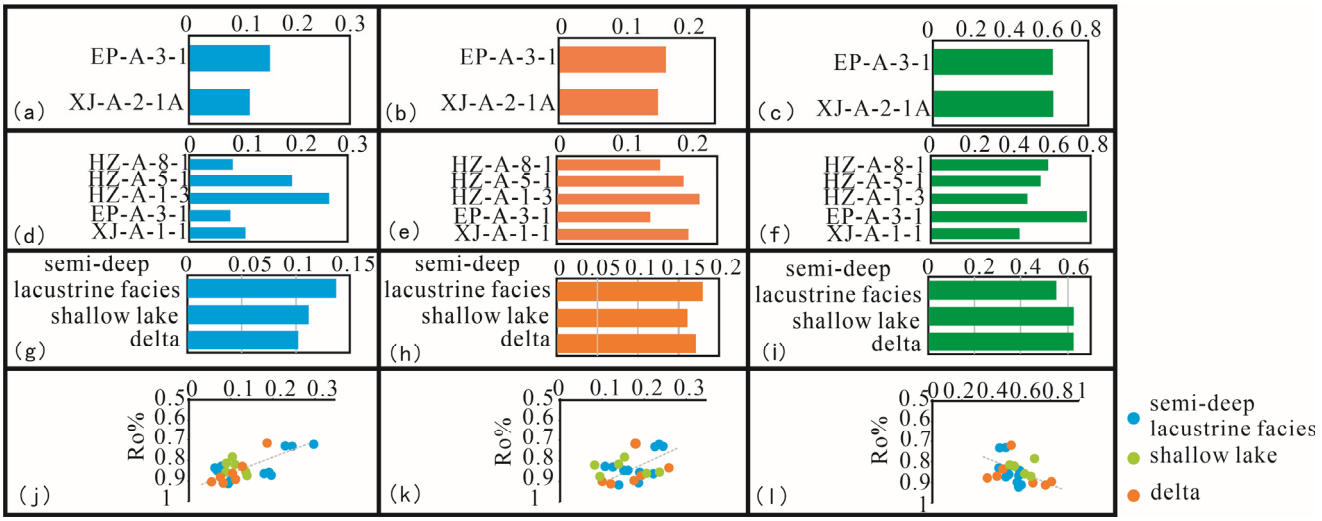


Figure 9. Infrared spectrum characteristics of hydrocarbon source rocks in the Zhu-1 Depression. ((**a**), Enping formation fatness parameter map; (**b**), Enping formation branching degree parameter map; (**c**), Enping formation aroma parameter map; (**d**), Wenchang formation fatness parameter map; (**e**), Wenchang formation branching degree parameter map; (**f**), Wenchang formation aroma parameter; (**g**), relationship diagram of parameters of the fatness; (**h**), relationship diagram of the branching degree parameter; (**i**), relationship diagram of the aroma parameter; (**j**), relationship diagram of fatness parameters; (**k**), relationship diagram of the branching degree parameter; (**l**), relationship diagram of the aroma parameter).

5.4. Summary

The development of organic matter in lacustrine hydrocarbon source rocks is controlled at the microscopic level by factors such as light intensity, nutrient supply, terrestrial organic matter input, abundance of self-generated algae in lakes, content of self-generated bacteria, redox status of sedimentary water media, water salinity, basin stability, clay mineral content, and sediment deposition rate. In summary, these factors affect organic matter production, preservation, and dilution. Macroscopically, the sedimentation of lacustrine hydrocarbon source rocks is controlled by tectonic activity and climatic conditions: tectonic activity creates the basin's accommodating space, provides the most basic conditions for the formation of hydrocarbon source rocks, controls the geometric shape such as the slope of the lake basin, and thus affects the stability of the lake basin. Climate conditions control the depth of lake water, the composition of lake productivity, and the type of

surface sediment weathering. The sedimentation rate controls the preservation or dilution of organic matter. The sedimentary periods of the Wenchang Formation and Enping Formation source rocks have different structural and climatic conditions, leading to changes in productivity and sedimentary water environment, which are well recorded in organic and inorganic geochemical parameters.

Tectonic activities not only formed the marginal shallow lake facies II_2-III, which are primarily characterized by the poor to medium quality of the Enping Formation and the semi-deep lake facies II_1 dominated by the good to very good quality of the Wenchang Formation but also caused a shift in the sedimentary center. This shift led to stratigraphic changes between the late Wenchang and Enping periods, affecting the quality and distribution of hydrocarbon source rocks. The depositional environments for source rocks during the Wenchang and Enping periods were vastly different. Compared to the Enping period, the Wenchang period experienced higher temperatures, lower humidity, higher initial productivity in the lake basins, and more saline water bodies. Research indicates that the source rocks in the Zhu-1 Depression were significantly influenced by ancient oxygen conditions, which directly affected the preservation of organic matter. The ratios of V/(V + Ni) and V/Cr are effective in indicating the redox conditions of the water body and show a good correlation with TOC. In addition, the hydrocarbon-generating aliphatic structures in the Wenchang Formation exceed those in the Enping Formation. Combined with micro-component analysis, the hydrocarbon products of the Wenchang Formation are crude oil and wet gas + condensate, while those of the Enping Formation are wet gas + condensate.

Therefore, it can be demonstrated that the Wenchang Formation's source rocks are the primary hydrocarbon source rocks in the Zhu-1 Depression, with a greater contribution to hydrocarbon generation than those of the Enping Formation. Paleo-redox, as a condition for the preservation of organic matter, controlled the development of source rocks.

6. Conclusions

(1) The Wenchang Formation's hydrocarbon source rocks, characterized by semi-deep lacustrine facies, boast a high abundance of organic matter, predominantly type II_1, with excellent to very good quality. These rocks constitute the primary hydrocarbon source for the early oil and late gas phases in the lacustrine facies of the Zhu-1 Depression. Conversely, the hydrocarbon source rocks of the Enping Formation, characterized by limnetic facies, predominantly consist of type II_2-III organic matter with varying qualities ranging from poor to medium. Nevertheless, they remain significant contributors to both oil and gas reserves in the region.

(2) Over the transition from the Wenchang to the Enping period, the climate shifted from warm and arid to cool and humid. The prevailing climate trended towards a freshwater environment with weakly oxidizing to weakly reducing conditions, resulting in a gradual decrease in paleo-productivity.

(3) The enrichment of organic matter in the hydrocarbon source rocks of the Enping and Wenchang Formations within the Zhu-1 Depression was largely controlled by paleo-oxygenation facies. The ratio of V/(V + Ni) to V/Cr serves as a reliable indicator of the water's redox environment, exhibiting a strong correlation with Total Organic Carbon (TOC) levels.

(4) In comparison to the hydrocarbon source rocks of the limnetic facies found in the Enping Formation, those from the semi-deep lacustrine facies in the Wenchang Formation exhibit a higher hydrocarbon-yielding aliphatic structure. Conversely, the aromatic hydrocarbon structure, with lower hydrocarbon potential, is less prominent in the Wenchang Formation compared to the Enping Formation.

(5) Source rocks from the Wenchang Formation's semi-deep lacustrine facies display a higher content of sapropel group + exinite group, indicating superior hydrocarbon generation potential. Conversely, the source rocks of the limnetic facies within the Enping Formation demonstrate a lower content of sapropelite + exinite with considerable variation, suggesting an average oil and gas generation potential.

Author Contributions: Software, Y.S.; Data curation, Y.S., W.X. and S.N.; Writing—original draft, J.Z.; Writing—review & editing, G.X.; Project administration, G.X. All authors have read and agreed to the published version of the manuscript.

Funding: National Major Science and Technology Project, "Optimal Selection and Favorable Exploration Direction Prediction of China's Offshore Oil rich Depression" (2016ZX05024002).

Data Availability Statement: Data are contained within the article.

Conflicts of Interest: Yuling Shi, Wanlin Xiong and Shengli Niu are from CNOOC (China) Co., Ltd., Shenzhen Branch, China. The authors declare no conflict of interest.

References

1. Kelts, K. Environments of Deposition of Lacustrine Petroleum Source Rocks: An Introduction. *Geol. Soc. Lond. Spec. Publ.* **1988**, *40*, 3–26. [CrossRef]
2. Wei, H.; Chen, D.; Wang, J.; Yu, H.; Tucker, M.E. Organic accumulation in the lower Chihsia Formation (Middle Permian) of South China: Constraints from pyrite morphology and multiple geochemical proxies. *Palaeogeogr. Palaeoclimatol. Palaeoecol.* **2012**, *353–355*, 73–86. [CrossRef]
3. Rimmer, S.M.; Thompson, J.A.; Goodnight, S.A.; Robl, T.L. Multiple controls on the preservation of organic matter in Devonian-Mississippian marine black shales: Geochemical and petrographic evidence. *Palaeogeogr. Palaeoclimatol. Palaeoecol.* **2004**, *215*, 125–154. [CrossRef]
4. Ingall, E.D.; Cappellen, P.V. Relation between sedimentation rate and burial of organic phosphorus and organic carbon in marine sediments. *Geochim. Cosmochim. Acta* **1990**, *54*, 373–386. [CrossRef]
5. Huang, B.; Xiao, X.; Zhang, M. Geochemistry, grouping and origins of crude oils in the Western Pearl River Mouth Basin, offshore South China Sea. *Org. Geochem.* **2003**, *34*, 993–1008. [CrossRef]
6. Ye, Q. The Late Mesozoic Structure Systems in the Northern South China Sea Margin: Geodynamics and Their Influence on the Cenozoic Structures in the Pearl River Mouth Basin. Ph.D. Thesis, China University of Geosciences, Wuhan, China, 2019.
7. Liu, H. Rift Style Controlled by Basement Attribute and Regional Stress in Zhu I Depression, Pearl River Mouth Basin. Ph.D. Thesis, China University of Geosciences, Wuhan, China, 2018.
8. Liu, P.; Zhang, X.; Du, J.; Chen, W.; Tao, W.; Tao, Y. Techonic-Thermal Evolution Process and the Petroleum Geological Significance of Relatively Low Geothermal Gradient in a Rift Basin: An Example from Xijiang Main Sag in Pearl River Mouth Basin. *Geol. Sci. Technol. Inf.* **2018**, *37*, 149–156. [CrossRef]
9. Mi, L.; Zhang, X.; Pang, X.; Zheng, J.; Zhang, L. Formation mechanism and petroleum geology of Pearl River Mouth basin. *Acta Pet. Sin.* **2019**, *40* (Suppl. S1), 1–10. [CrossRef]
10. Deng, P. The Nature and Tectonic Transition of the Multiphase Rifting in the Northern Margin of the South China Sea: Based on the Study of the Zhu I Depression in Pearl River Mouth Basin. Ph.D. Thesis, China University of Geosciences, Wuhan, China, 2018.
11. Wu, J. Enrichment Regularity of Zhu I Depression, Pearl River Mouth Basin. Ph.D. Thesis, China University of Geosciences, Wuhan, China, 2013.
12. Bao, J.; Chen, C.; Zhu, C. Novel C15 sesquiterpanes and their origin in different crude oils from the Pearl River Mouth Basin of China. *Sci. China Earth Sci.* **2016**, *59*, 1622–1632. [CrossRef]
13. Fu, N.; Zhu, L. Research on Mixed Oil in Western Huizhou Sag of Zhu I Depression. *China Pet. Explor.* **2007**, *2*, 20–26+83.
14. Zhu, Y.; Xie, J.; Sun, L.; Hao, F.; Zhu, J. Identification and geochemical significances of novel bicyclic and tetracyclic terpanes in crude oils from the Pearl River Mouth Basin. *Geochimica* **2015**, *44*, 313–322. [CrossRef]
15. Zhu, J.; Shi, H.; Yu, S.; Du, J.; Luo, J. Heating and Pressing simulation Experiments of Typical source rocks of Zhu I Depression--Discussion of modes of Hydrocarbon Generation and Expellation and TOC Recovery Coefficients. *Nat. Gas Geosci.* **2006**, *4*, 573–578.
16. Shi, H.; Zhu, J.; Jiang, Z.; Yu, S.; Xie, T.; Wu, J. Hydrocarbon resources reassessment in Zhu I Depression, Pearl River Mouth Basin. *China Offshore Oil Gas* **2009**, *21*, 9–14.

17. *GB/T 19145-2003*; Determination of Total Organic Carbon in Sedimentary Rock. Standards Press of China: Beijing, China, 2003.
18. *GB/T 18602-2012*; Rock Pyrolysis Analysis. Standards Press of China: Beijing, China, 2012.
19. *GB/T 14506.14-2010*; Methods for Chemical Analysis of Silicate Rocks—Part 14: Determination of Ferrous Oxide Content. Standards Press of China: Beijing, China, 2010.
20. *GB/T 14506.30-2010*; Methods for Chemical Analysis of Silicate Rocks—Part 30: Determination of 44 Elements. Standards Press of China: Beijing, China, 2010.
21. Arthur, M.A.; Jenkyns, H.C.; Brumsack, H.J.; Schlanger, S.O. Stratigraphy, geochemistry, and paleoceanography of organic-carbon rich Cretaceous sequences. In *Cretaceous Research, Events and Rhythms*; Ginsburg, R.N., Beaudoin, B., Eds.; Kluwer Academic: Norwell, MA, USA, 1990; pp. 75–119. [CrossRef]
22. Morford, J.L.; Russell, A.D.; Emerson, S. Trace metal evidence for changes in the redox environment associated with the transition from terrigenous clay to diatomaceous sediment, Saanich Inlet, BC. *Mar. Geol.* **2001**, *174*, 355–369. [CrossRef]
23. Algeo, T.J.; Maynard, J. Trace-element behavior and redox facies in core shales of Upper Pennsylvanian Kansas-type cyclothems. *Chem. Geol.* **2003**, *206*, 289–318. [CrossRef]
24. Taylor, S.R.; McLennan, S.M. *The Continental Crust: Its Composition and Evolution*; Blackwell Scientific Publication: Oxford, UK, 1985.
25. Algeo, T.J.; Tribovillard, N. Environmental analysis of paleoceanographic systems based on molybdenum-uranium covariation. *Chem. Geol.* **2009**, *268*, 211–225. [CrossRef]
26. Peters, K.E. Guidelines for evaluating petroleum source rock using programmed pyrolysis. *AAPG* **1986**, *70*, 318–329. [CrossRef]
27. Zhu, M.; Zhang, X.; Huang, Y.; Zhu, J.; Long, Z.; Shi, Y.; Shi, C.; Zhang, X. Source rock characteristics and resource potential in Pearl River Mouth Basin. *Acta Pet. Sin.* **2019**, *40*, 53–68. [CrossRef]
28. Tissot, B.P.; Welte, D.H. *Petroleum Formation and Occurrence*, 2nd ed.; Springer: Berlin/Heidelberg, Germany; New York, NY, USA; Tokyo, Japan, 1984.
29. Qin, J. *Hydrocarbon Source Rocks in China*; Science Press: Beijing, China, 2005.
30. Ruan, J.; Bai, W. Analysis and Application of Infra-rad Spectra for Kerogen. *Exp. Pet. Geol.* **1988**, *1*, 80–86.
31. Teichmüller, M. Organic petrology of source rocks, history and state of the art. *Org. Geochem.* **1986**, *10*, 581–599. [CrossRef]
32. Fedo, C.M.; Nesbitt, H.W.; Young, G.M. Unraveling the effects of potassium metasomatism in sedimentary rocks and paleosols, with implications for paleoweathering conditions and provenance. *Geology* **1995**, *23*, 921–924. [CrossRef]
33. Xie, Y.; Wu, F.; Fang, X. A major environmental shift by the middle Eocene in southern China: Evidence from palynological records. *Rev. Palaeobot. Palynol.* **2020**, *278*, 104226. [CrossRef]
34. Zheng, R.; Liu, M. Study on Palaeosalinity of Chang-6 Oil Reservoir set in Ordos Basin. *Oil Gas Geol.* **1999**, *1*, 22–27.
35. Berner, R.A.; Raiswell, R. C/S method for distinguishing freshwater from marine sedimentary rocks. *Geology* **1984**, *12*, 365–368. [CrossRef]
36. Chen, J.; Zhao, L.; Algeo, T.J.; Zhou, L.; Zhang, L.; Qiu, H. Evaluation of paleomarine redox conditions using Mo-isotope data in low-[Mo] sediments: A case study from the lower Triassic of South China. *Palaeogeogr. Palaeoclimatol. Palaeoecol.* **2019**, *519*, 178–193. [CrossRef]
37. Zhai, L.; Wu, C.; Ye, Y.; Zhang, S.; An, Z. Marine redox variations during the Ediacaran–Cambrian transition on the Yangtze Platform, South China. *Geol. J.* **2018**, *53*, 58–79. [CrossRef]
38. Bertine, K.K.; Turekian, K.K. Molybdenum in marine deposits. *Geochim. Cosmochim. Acta* **1973**, *37*, 1415–1434. [CrossRef]
39. Kashiwabara, T.; Takahashi, Y.; Tanimizu, M. A XAFS study on the mechanism of isotopic fractionation of molybdenum during its adsorption on ferromanganese oxides. *Geochem. J.* **2011**, *43*, 31–36. [CrossRef]
40. Zheng, Y.; Anderson, R.F.; Geen, A.V.; Fleisher, M.Q. Remobilization of authigenic uranium in marine sediments by bioturbation. *Geochim. Cosmochim. Acta* **2002**, *66*, 1759–1772. [CrossRef]
41. Helz, G.R.; Miller, C.V.; Charnock, J.M.; Mosselmans, J.F.W.; Pattrick, R.A.D.; Garner, C.D.; Vaughan, D.J. Mechanism of molybdenum removal from the sea and its concentration in black shales: EXAFS evidence. *Geochim. Cosmochim. Acta* **1996**, *60*, 3631–3642. [CrossRef]
42. Tribovillard, N.; Averbuch, O.; Devleeschouwer, X.; Racki, G.; Riboulleau, A. Deep-water anoxia over the frasnian–famennian boundary (la serre, france): A tectonically induced oceanic anoxic event? *Terra Nova* **2004**, *16*, 288–295. [CrossRef]
43. Wu, M.; Ouyang, Z. Cerium anomaly: A chemical tracer for tracing changes in redox conditions in ancient oceans. *Chin. Sci. Bull.* **1992**, *3*, 242–244.
44. Department of Marine Geology, Tongji University. *Introduction to Ancient Oceanography*; Tongji University Publishing House: Shanghai, China, 1989; pp. 1–20.
45. Wei, H. Productivity and redox proxies of palaeo-oceans: An overview of elementary geochemistry. *Sediment. Geol. Tethyan Geol.* **2012**, *32*, 76–88.
46. Myrbo, A.; Shapley, M.D. Seasonal water-colum dynamics of dissolved inorganic carbon stable isotopic composition in small hard water lakes in Minnesota and Montana. *Geochim. Cosmochim. Acta* **2006**, *70*, 2699–2714. [CrossRef]

47. Muller, P.J.; Suess, E. Productivity, sedimentation rate and sedimentary organic matter in the oceans—I. Organic carbon preservation. *Deep Sea Res.* **1979**, *26*, 1347–1362. [CrossRef]
48. Mix, A.C. Pleistocene paleoproductivity evidence from organic carbon and foraminiferal species. In *Productivity of the Ocean: Present and Past*; Berger, W.H., Ed.; John Wiley Sons Press: New York, NY, USA, 1989; pp. 313–340.
49. He, J.; Ding, W.; Jiang, Z.; Jiu, K.; Li, A.; Sun, Y. Mineralogical and chemical distribution of the Es3L oil shale in the Jiyang Depression, Bohai Bay Basin (E China): Implications for paleoenvironmental reconstruction and organic matter accumulation. *Mar. Pet. Geol.* **2017**, *81*, 196–219. [CrossRef]
50. Li, L.; Liu, Z.J.; George, S.C.; Sun, P.C.; Xu, Y.B.; Meng, Q.T.; Wang, K.B.; Wang, J.X. Lake evolution and its influence on the formation of oil shales in the Middle Jurassic Shimengou Formation in the Tuanyushan area, Qaidam Basin, NW China. *Geochemistry* **2019**, *79*, 162–177. [CrossRef]
51. Kuss, J.; Kremling, K. Particulate trace element fluxes in the deep northeast Atlantic Ocean. *Deep-Sea Res. Part I* **1999**, *46*, 149–169. [CrossRef]
52. Pohl, C.; Loffler, A.; Hennings, U. A sediment trap flux study for trace metals under seasonal aspects in the stratified Baltic Sea (Gotland Basin: 57° 19.20′ N; 20° 03.00′ E). *Mar. Chem.* **2004**, *84*, 143–160. [CrossRef]
53. Riboulleau, A.; Baudin, F.; Deconinck, J.F.; Derenne, S.; Largeau, C.; Tribovillard, N. Depositional conditions and organic matter preservation pathways in an epicontinental environment: The Upper Jurassic Kashpir Oil Shales (Volga Basin, Russia). *Palaeogeogr. Palaeoclimatol. Palaeoecol.* **2003**, *197*, 171–197. [CrossRef]
54. Cao, T. Element Geochemistry Evaluation of Marine Source Rock with High Maturity: A Case Study of Lower Cambrian in Yangba Section of Nanjiang County, Sichuan. Master's Thesis, China University of Geosciences, Wuhan, China, 2011.
55. Dymond, J.; Suess, E.; Lyle, M. Barium in Deep-Sea Sediment: A Geochemical Proxy for Paleoproductivity. *Paleoceanography* **1992**, *7*, 163–181. [CrossRef]
56. Nürnberg, C.C.; Bohrmann, G.; Schlüter, M.; Frank, M. Barium accumulation in the Atlantic sector of the Southern Ocean: Results From 190,000-year records. *Paleoceanography* **1997**, *12*, 594–603. [CrossRef]
57. Murphy, A.E.; Sageman, B.B.; Hollander, D.J.; Lyons, T.W. Black shale deposition and faunal overturn in the Devonian Appalachian Basin: Clastic starvation, seasonal water-column mixing, and efficient biolimiting nutrient recycling. *Paleoceanography* **2000**, *15*, 280–291. [CrossRef]
58. Zhang, L. The Progress On The Study Of Lacustrine Source Rocks. *Pet. Geol. Exp.* **2008**, *30*, 591–595.
59. Li, Y.; Shao, D.; Lv, H.; Zhang, Y.; Zhang, X.; Zhang, T. A relationship between elemental geochemical characteristics and organic matter enrichment in marine shale of Wufeng Formation-Longmaxi Formation, Sichuan Basin. *Acta Pet. Sin.* **2015**, *36*, 1470–1483. [CrossRef]
60. Jones, B.; Manning, D. Comparison of geochemical indices used for the interpretation of palaeoredox conditions in ancient mudstones. *Chem. Geol.* **1994**, *111*, 111–129. [CrossRef]
61. Hatch, J.R.; Leventhal, J.S. Relationship between inferred redox potential of the depositional environment and geochemistry of the Upper Pennsylvanian (Missourian) Stark Shale Member of the Dennis Limestone, Wabaunsee County, Kansas, U.S.A. *Chem. Geol.* **1992**, *99*, 65–82. [CrossRef]
62. Bruland, K.W. Trace elements in sea-water. In *Chemical Oceanography*; Riley, J.P., Chester, R., Eds.; Academic Press: London, UK, 1983; pp. 157–220.
63. Klinkhammer, G.P.; Palmer, M.R. Uranium in the oceans: Where it goes and why. *Geochim. Cosmochim. Acta* **1991**, *55*, 1799–1806. [CrossRef]
64. Francois, R. A study of the regulation of the concentration of some trace metals (Rb, Sr, Zn, Pb, Cu, V, Cr, Ni, Mn, Mo) in Sannich Inlet sediments, British Columbia, Canada. *Mar. Geol.* **1988**, *83*, 285–308. [CrossRef]
65. Anderson, R.F.; Fleisher, M.Q.; LeHuray, A.P. Concentration, oxidation state, and particulate flux of uranium in the black sea. *Geochim. Cosmochim. Acta* **1989**, *53*, 2215–2224. [CrossRef]
66. Crusius, J.; Calvert, S.; Pedersen, T.; Sage, D. Rehenium and molybdenum enrichments in sediments as indicators of oxic, suboxic, and sulfidic conditions of deposition. *Earth Planet. Sci. Lett.* **1996**, *145*, 65–78. [CrossRef]
67. Calvert, S.E.; Pedersen, T.F. Geochemistry of recent oxic and anoxic marine sediments: Implications for the geological record. *Mar. Geol.* **1993**, *113*, 67–88. [CrossRef]
68. Hild, E.; Brumsack, H.J. Major and minor element geochemistry of Lower Aptian sediments from the NW German Basin (core Hoheneggelsen KB 40). *Cretac. Res.* **1998**, *19*, 615–633. [CrossRef]
69. Hastings, D.W.; Emerson, S.R.; Mix, A.C. Vanadium in foraminiferal calcite as a tracer for changes in the areal extent of reducing sediments. *Paleoceanography* **1996**, *11*, 665–678. [CrossRef]
70. Calvert, S.E.; Piper, D.Z. Geochemistry of ferromanganese nodules from domes site a, northern equatorial pacific: Multiple diagenetic metal sources in the deep sea. *Geochim. Cosmochim. Acta* **1984**, *48*, 1913–1928. [CrossRef]
71. Whitfield, M. Interactions between phytoplankton and trace metals in the ocean. *Adv. Mar. Biol.* **2001**, *41*, 1–128.

72. Piper, D.Z.; Perkins, R.B. A modern vs. Permian black shale—The hydrography primary productivity and water-column chemistry of deposition. *Chem. Geol.* **2004**, *206*, 177–197. [CrossRef]
73. Tribovillard, N.; Algeo, T.J.; Lyons, T.; Riboulleau, A. Trace metals as paleoredox and paleoproductivity proxies: An update. *Chem. Geol.* **2006**, *232*, 12–32. [CrossRef]
74. Nameroff, T.J.; Calvert, S.E.; Murray, J.W. Glacial-interglacial variability in the eastern tropical north pacific oxygen minimum zone recorded by redox-sensitive trace metals. *Paleoceanography* **2004**, *19*, PA1010. [CrossRef]
75. Chang, H.; Chu, X.; Feng, L.; Huang, J.; Zhang, Q. Redox sensive Trace Elements as Plaleoenviroments Proxies. *Geol. Rev.* **2009**, *55*, 91–99. [CrossRef]
76. Zhang, X.; Yan, X.; Li, P.; Miao, D.; Hu, W.; Liu, Q. The Method of Determination of Aliphatic Content in Kerogen by Quantitative FT-IR and Its Petroleum Geology Significance. *Acta Sedimentol. Sin.* **2004**, *4*, 711–717. [CrossRef]
77. Ma, X.; Ran, Y. Simulation and characterization of thermal evolution of kerogen in Maoming oil shale. *Geochimica* **2013**, *42*, 373–378. [CrossRef]
78. Wang, Q.; Xu, X.; Chi, M.; Zhang, H.; Cui, D.; Bai, J. FT-IR study on composition of oil shake kerogen and its pyrolysis oil generation characteristics. *J. Fuel Chem. Technol.* **2015**, *43*, 1158–1166.
79. Lu, L.; Cai, J.; Liu, W.; Teng, G.; Hu, W. Infra-red emission spectroscopy study of thermal evolution of organic matter bound by clay minerals in muddy hydrocarbon source rocks. *Pet. Geol. Exp.* **2012**, *34*, 215–222.

Disclaimer/Publisher's Note: The statements, opinions and data contained in all publications are solely those of the individual author(s) and contributor(s) and not of MDPI and/or the editor(s). MDPI and/or the editor(s) disclaim responsibility for any injury to people or property resulting from any ideas, methods, instructions or products referred to in the content.